6-3-1959

A Study of the Radioactive Decay of the Two Isomers of Pd109 and of the Associated Low-Lying Levels of Ag109

John W. Starner

A STUDY OF THE RADIOACTIVE DECAY - STARNER

A STUDY OF THE RADIOACTIVE DECAY OF THE TWO ISOMERS OF Pd^{109} AND OF THE ASSOCIATED LOW-LYING LEVELS OF Ag^{109}

By

John W. Starner

A Thesis

Submitted in Partial Fulfillment of the

Requirements for the Degree of

Master of Science in Physics

The University of New Mexico

1959

This thesis, directed and approved by the candidate's committee, has been accepted by the Graduate Committee of the University of New Mexico in partial fulfillment of the requirements for the degree of

MASTER OF SCIENCE

E. A. Castetter

DEAN

June 3, 1959

DATE

Thesis committee

Raul Froman

CHAIRMAN

Jack Katzenstein

Nolan Jamie

Merle E. Bunker

ABSTRACT

The radiations of Pd^{109} (13.45 ± 0.01 hr) and Pd^{109m} (4.69 ± 0.01 min) have been investigated with a coincidence scintillation spectrometer and a solenoidal beta-ray spectrometer. Pd^{109m} was observed to have only one mode of decay: a 188-kev (E3) isomeric transition to Pd^{109}. The principal beta-ray group (>99.9%) of Pd^{109} was found to have an end-point energy of 1.025 ± 0.005 Mev. Gamma rays of the following energies (kev) and approximate intensities (photons/10^5 disintegrations) were observed to accompany the decay of Pd^{109}: 773 (4), 707 (2), 643 (10), 602 (2), 553 (2), 448 (1), 412 (10), 325 (0.5), 307 (10), 129 (0.5), 88 (6×10^3), and 41 (1). The following gamma-gamma coincidences were observed: 643-129, 602-129, 602-41, 553-307, 448-412, 412-307 kev. A level scheme is proposed for Ag^{109} which involves energy levels at 88, 129, 307, 412, 719, 732, and 860 kev.

ACKNOWLEDGMENTS

The author is greatly indebted to Dr. Merle E. Bunker for suggesting this project and for rendering invaluable advice and assistance. Thanks are also extended to Mrs. Almera L. Turner for typing the manuscript. The author is grateful to the Los Alamos Scientific Laboratory for support during the course of this work.

CONTENTS

LIST OF FIGURES

LIST OF TABLES

CHAPTER I

INTRODUCTION

Experimental physicists have used two fundamentally different methods of approach to obtain a consistent picture of the atomic nucleus. One method is to study the elementary particles, their properties, and their interactions. From the observed two-body reactions information is obtained on the fundamental nuclear forces which can be applied to the infinitely more complicated many-body atomic nuclei. The other method is to obtain all possible nuclear data and to examine the relationships among these data. One expects to find a large number of correlations indicating the existence of elementary laws of nuclear structure. Theoretical interpretation of the complimentary information obtained from these two methods of approach has led to an improved, but still incomplete, understanding of nuclear structure.

A physicist following the second method of approach is invariably led to examine accumulated data in the light of a model. As there is great diversity in the phenomena investigated, it is only natural that different models should emerge for systemmatizing the data observed. One fruitful field of endeavor has been the study of the decay of radioactive nuclei. From these studies a large collection of data has been obtained on spins, parities, and energies of nuclear states and on β- and γ-ray transition rates.

During the last decade, two particularly successful models have been developed to explain this type of data. The first of these two models to appear was the Shell Model[1,2,+] which, though postulated prior to 1930, was not developed into a usable model until after 1950. The assumptions on which this model is based are that the nucleons move nearly independently in a common static spherical

---

[+] Superscript numbers in the text refer to items so numbered in the List of References, infra.

potential, that the more tightly bound nucleons couple to form closed shells of zero angular momentum, and that the coupling between the more loosely bound nucleons determines the specific nuclear properties. Because of the assumption of a spherical potential, it is immediately evident that this model should be most successful in the vicinity of closed shells of both neutrons and protons. In these regions, excellent agreement has indeed been observed between calculated and experimentally determined values of a large variety of nuclear properties. In regions somewhat removed from double-closed shells the nuclear potential is no longer spherical, so the model, while still successful in explaining isomerism and ground-state spins and parities, now is only qualitative in explaining level ordering and transition rates. For the regions $155 \leq A \leq 181$ and $A \geq 227$, the nuclei are so highly deformed that the shell model essentially fails.

The second useful model is the Collective Model.[3,4] The assumptions underlying this model are that the nucleons move nearly independently in a common, slowly varying, noncentral potential and that the nuclear shape remains invariant. The nuclear motion will then separate into individual-particle and rotational motions. This model is of greatest value in the regions $155 \leq A \leq 181$ and $A \geq 227$ where the nuclei are highly deformed. In these regions, the collective model makes specific predictions about the existence and properties of rotational states. Remarkable agreement has been observed between theory and experiment, particularly regarding the rotational-level energies and γ-ray transition rates.

In regions where the nucleus is only slightly deformed, neither model is adequate and some features of each appear. One such region where this appears to be the case is that of odd-even nuclei with $40 < Z < 50$. In this region, ground-state spins and paraties and all known cases of isomerism are satisfactorily explained by the shell model. However, the collective model is required to account for the rotational states observed[5] in the three stable nuclides Rh^{103}, Ag^{107}, and Ag^{109}.

A theoretical interpretation of the level structure of the odd-even nuclides in this region can be made only when adequate experimental information becomes available. There are three principal ways to obtain this information: coulomb excitation studies, neutron inelastic scattering studies, and studies of the decay of radioactive nuclei. The stable nuclides in this region (Nb^{93}, Rh^{103}, Ag^{107}, Ag^{109}, In^{113}, and In^{115}) can be studied by Coulomb excitation and neutron inelastic scattering. Many high-quality coulomb excitation studies of these nuclides have been made[5,6,7] in which the bombarding particles used were protons and alpha particles. From these experiments considerable information has been obtained about certain low-lying states and their γ-ray decay probabilities. However, little new information is expected from this line of endeavor until higher-Z bombarding particles are used. Several studies[6] have been made of the γ rays emitted accompanying the inelastic scattering of neutrons from these nuclides. However, very little information has been obtained about the levels in Rh^{103}, and no usable information has been obtained about the levels in Ag^{107} and Ag^{109}. This latter situation will not be remedied until these experiments can be conducted with separated silver isotopes. The decay schemes[6] of most of the radioactive nuclei in this region are either incomplete or only partially understood and therefore still represent a fertile field of investigation. One of the least understood nuclides is Ag^{109}. The object of this research is to study the decay of Pd^{109m} and Pd^{109} toward obtaining all possible information about the energy levels of the nucleus Ag^{109}.

CHAPTER II

FUNDAMENTAL CONCEPTS USED IN NUCLEAR SPECTROSCOPY

2.1 The Shell Model.[1,2] The nuclear shell model is analogous to the orbital description of the electronic shells of the atom. The principle assumption made is that each nucleon moves in a static spherical potential created by the other nucleons. Agreement between the observed and calculated level sequence is obtained if the potential chosen is a square well plus a strong spin-orbit coupling term. The level sequence for protons, calculated on the basis of such a potential, is shown in Fig. 1. The calculated level sequence is essentially the same for neutrons and protons. The empirical evidence strongly suggests that neutrons and protons independently fill their own shells. Thus, any nucleus (Z,A) in the state of lowest energy will presumably have its Z protons in the Z lowest energy states available and its (A - Z) neutrons also in their lowest energy states. The spins of the neutrons and protons are assumed to couple independently by j-j coupling to form an effective neutron core spin, $\vec{J}_n$, and an effective proton core spin, $\vec{J}_p$. The nuclear spin, I, is then formed by $I = J = |\vec{J}_p + \vec{J}_n|$. For nuclear ground states the model predicts that pairs of identical nucleons couple to zero angular momentum; hence, neutron or proton cores with an even number of nucleons are expected to have zero spin, while cores with an odd number of nucleons are expected to have the spin of the odd nucleon. Empirically, it is found that every pair of identical nucleons increases the binding energy of the nucleus by an amount $\frac{25}{A}(2j + 1)$ Mev more than the sum of the individual-particle binding energies.[8]

Low-lying excited states of odd-A nuclei result from two quite different processes. The first is the excitation of the odd nucleon to a higher shell. The second is the recombination of the nucleons outside of closed shells to form

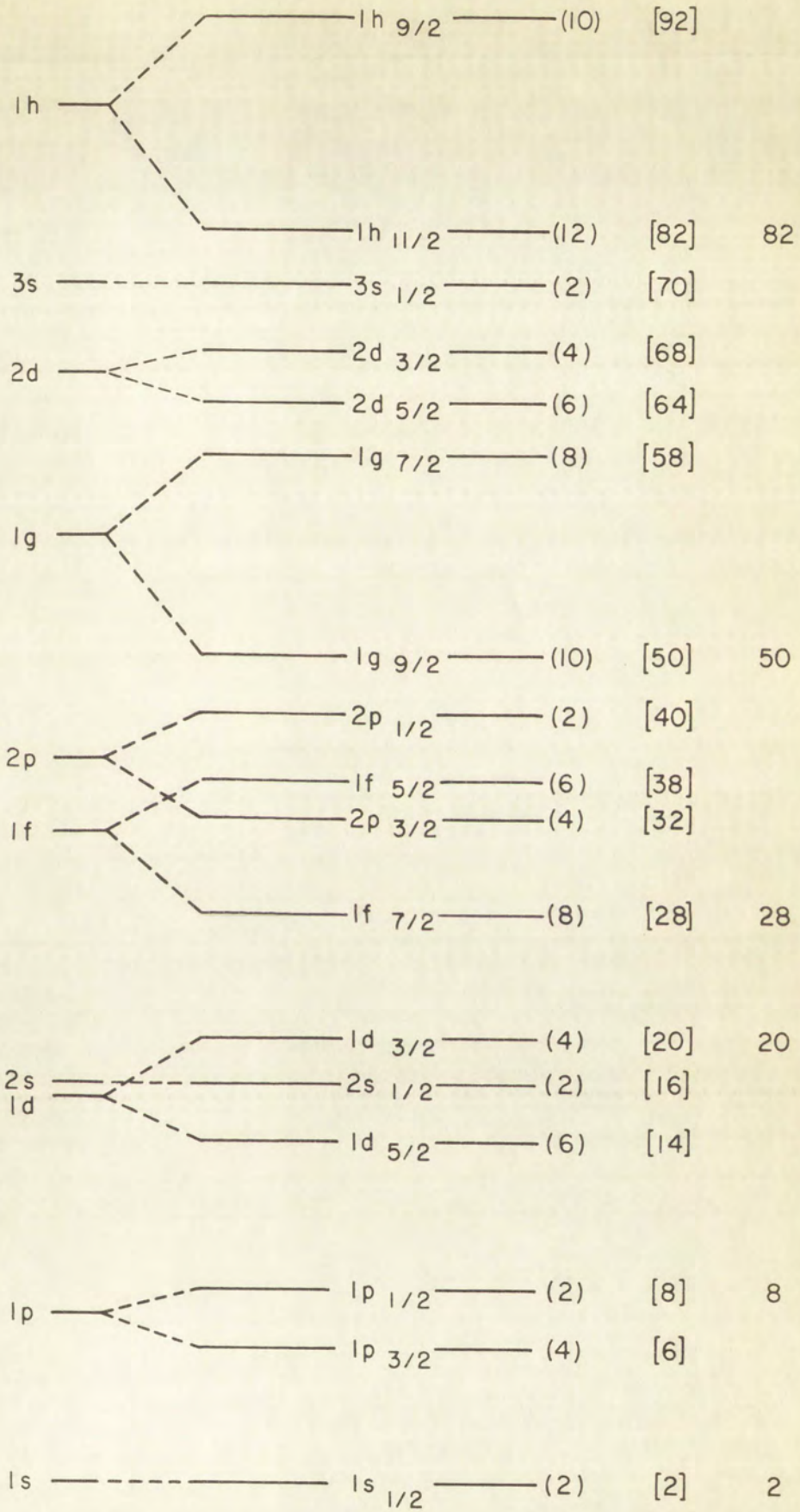

Fig. 1. Schematic representation of the level sequence for protons calculated using a spherically symmetric square well potential (shown at the left), and the semi-empirical sequence obtained by the addition of a spin-orbit splitting term to the square well potential.

The radial quantum number and symbol for the orbital angular momentum, like 2p, are written beside each level. The angular momentum value, $j = \ell \pm 1/2$, is written as a subscript, like $2p_{3/2}$. Numbers inside square brackets indicate total occupation numbers. The numbers at the far right, the so-called "magic" numbers, are the occupation numbers at levels where there is a large energy "jump" to the next shell.

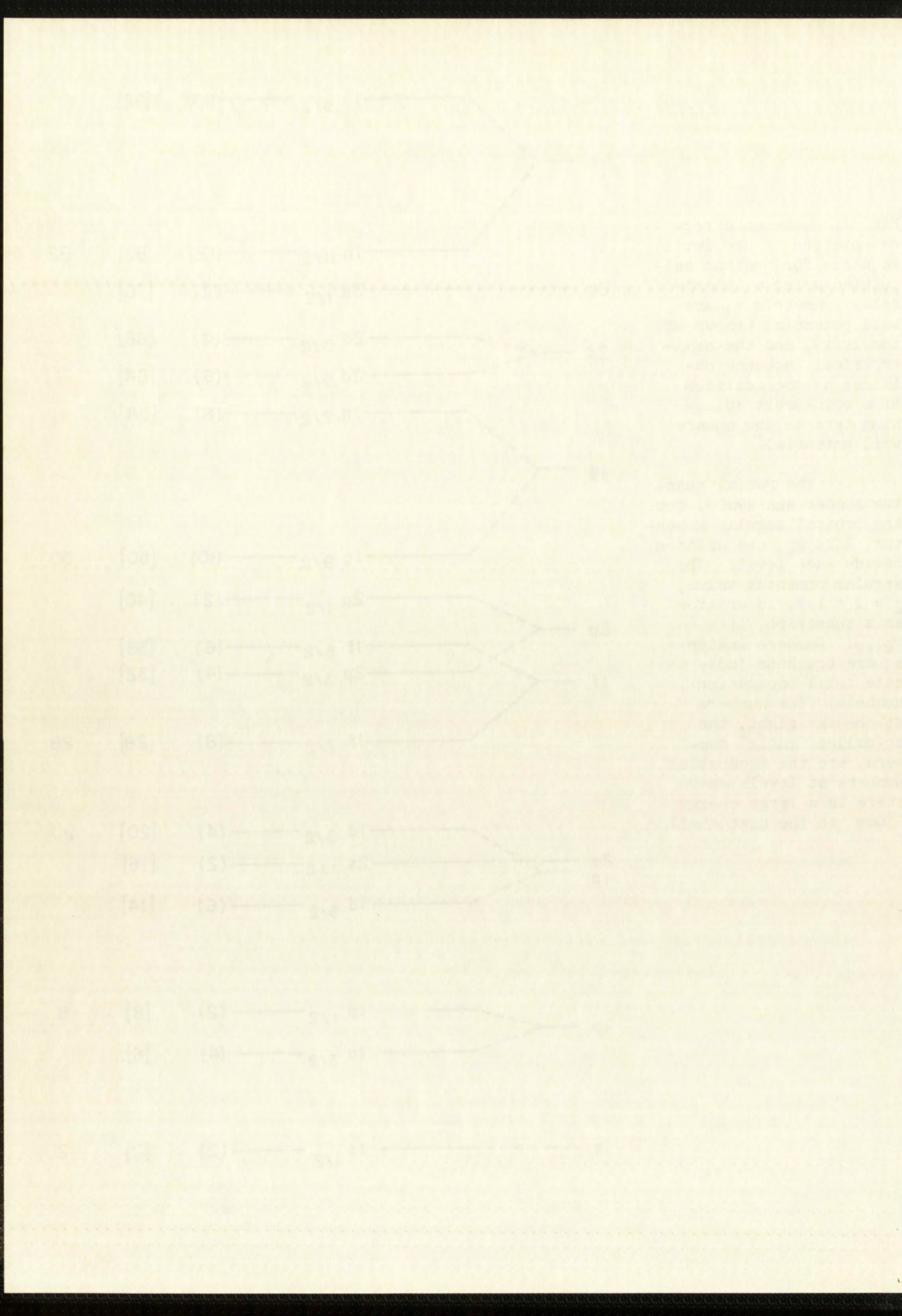

states having spins different from that of the last nucleon. The latter is responsible for more low-lying levels, as the average shell spacing is of the order of 1 Mev whereas level spacings due to recombinations of nucleons are a few hundred kilovolts.[9]

2.2 The Collective Model.[3,4] It is known that nuclei with many nucleons outside of closed shells are often highly deformed. The magnitude of most of the measured values of quadrupole moments for such nuclei can be explained only by the assumption of a large equilibrium deformation. The behavior of these deformed nuclei can be understood in terms of the Collective Model. This model describes the nucleus in terms of a coupled system of particle and collective degrees of freedom. In the limit of strong coupling the theory predicts that the nucleus will acquire a large axially-symmetric equilibrium deformation. The eigenfunctions of a system of nucleons moving in a dynamic spheroidal nucleus can be shown to have the form

$$\psi = X_p \, D_{rot} \, \phi_{vib}. \tag{2.1}$$

As a consequence of the separability of the eigenfunctions, the associated energy eigenvalues are

$$E = E_p + E_{rot} + E_{vib}. \tag{2.2}$$

The terms X_p and E_p can be considered to result from the independent motion of the nucleons in a static spheroidal potential. The terms D_{rot} and E_{rot} can be considered to result solely from the rotational motion of the nucleus, considered as fixed in shape. The terms ϕ_{vib} and E_{vib} can be considered to result

from the vibrational motion of the nucleus. The vibrational energies are in excess of 1 Mev, so are of no interest in this work and will be ignored. The rotational states of odd-A nuclei have energies (E_{rot}) given by the equation

$$E_{rot} = \frac{h^2}{2\mathcal{J}}[I(I+1) + a(-1)^{I+1/2}(I+1/2)\delta(K,1/2)] \qquad (2.3)$$

where the total angular momentum I has the sequence of values

$$I = I_o, I_o + 1, I_o + 2 \cdots \qquad (2.4)$$

and where a is the so-called decoupling parameter, K is the projection of I on the nuclear symmetry axis, and $\mathcal{J}$ is the effective moment of inertia about an axis perpendicular to the nuclear symmetry axis.

2.3 Beta Decay.[10,11] The theory of beta decay is sufficiently complicated that only certain pertinent facts and formulae will be stated here. The theory by which the energy spectrum and transition rates are calculated involves the evaluation of matrix elements between initial and final states. As in other quantum mechanical calculations, nonvanishing matrix elements result only from those transitions which obey certain selection rules. The selection rules obtained for "allowed" transitions are $\Delta I = 0, \pm 1$ and no change in parity between initial and final states. When these selection rules are violated, slower "forbidden" transitions occur. The occurrence of such transitions is considered to result from small effects regarded as negligible in the development of the theory of allowed decay. These effects, grouped in order of decreasing magnitude, result in 1st forbidden, 2nd forbidden, etc., transitions, with each of which are associated unique selection rules. These selection rules are listed in Table I.

Investigation of the energy spectrum of beta particles is a logical first step in the study of the energy-level structure of nuclides populated by beta decay. Resolution of a many-group spectrum into its components gives direct information as to the energy levels populated. Also, through the relative intensities of the component groups, inferences can be made as to changes of angular momentum and parity. In the theory of beta decay the formula[10]

$$\left[\frac{N(W)}{pWF(Z,W)}\right]^{1/2} = K\left[W_o - W\right] \tag{2.5}$$

is developed, where N(W) is the number of beta particles per unit energy interval, p and W are the electron momentum and energy, respectively, F(Z,W) is a correction due to electron screening, K is a constant, and W_o is, by definition, the beta transition energy. Equation (2.5) predicts that a plot of $[N(W)/pWF(Z,W)]^{1/2}$ against energy (W) will be a straight line, intersecting the abscissa at the so-called end-point energy, W_o. This prediction has been verified experimentally. One advantage of this type of plot, referred to as a Fermi-Kurie plot, is that it facilitates the analysis of a complex beta spectrum into its individual groups. To be more specific, if two or more beta groups are present, a departure from linearity will occur at the end-point energy of the most energetic internal group. A systematic analysis will resolve the composite spectrum into individual Fermi-Kurie plots for each of the groups present, from which can be obtained the relative intensities of the groups and their end-point energies. From the relative intensities of the groups and the observed half-life for beta decay, the partial half-life, t, for each group can be calculated. The formula for the comparative half life, ft, for allowed beta transitions is[10]

$$ft = \frac{B}{(1 - x)\left|M_F\right|^2 + x\left|M_{GT}\right|^2} \tag{2.6}$$

where B and x are universal constants, M_F and M_{GT} are the Fermi and Gamow-Teller matrix elements, respectively, and

$$f = f(Z,W_o) = \int_1^{W_o} pW(W_o - W)^2 F(Z,W)dW. \qquad (2.7)$$

Tables and nomographs[11] for the determination of $f(Z,W_o)$ have been published. As M_F and M_{GT} are of the same order of magnitude for allowed transitions,[10] all "allowed" ft values should be approximately equal. For each degree of forbiddenness similar arguments can be made, so that measured values of $\log_{10}ft$ are expected to group according to the degree of forbiddenness. This has been confirmed experimentally.[12] Nominal empirical values are listed in Table I. The "yes" and "no" entries in the third column signify whether there is or is not a change of parity ($\Delta\pi$) between the initial and final states.

TABLE I. Nomenclature and representative ft values for the various types of beta transitions.

Transition type	Spin change ΔI	Parity change $\Delta\pi$	$\log_{10}ft$
Super allowed	0	No	3.5
Allowed	0, ±1	No	4.2 - 6
1st Forbidden	0, ±1	Yes	6 - 8.5
1st Forbidden	±2	Yes	8.5 - 10
2nd Forbidden	±2, ±3	No	12 - 14
3rd Forbidden	±3, ±4	Yes	17 - 21

2.4 Multipole Radiation.[13,14] Practically all low-lying excited states of nuclei decay to lower states with simultaneous emission of γ rays or internal-conversion electrons. The gamma radiation is classified by multipole order L,

according to the angular momentum L (in units of $\hbar$) carried off by each quantum. In addition, for each multipole order there are two classes corresponding to "yes" or "no" change of parity between initial and final states. "Multipolarity" is the term used to specify both the parity class and multipole order of the gamma radiation. The radiation is commonly referred to as being of multipolarity (EL) or (ML) corresponding to the classical electric or magnetic 2^L pole radiations. Conservation laws impose selection rules on the possible multipolarities of γ-ray transitions between two specified states. As transition probabilities decrease very rapidly with increasing multipole order, only one multipolarity is expected to be involved in any particular transition. Mixed M1 + E2 transitions are, however, frequently found for transitions with $\Delta I = 1$, $\Delta\pi$ = "no". The selection rules are summarized in Table II:[13]

TABLE II. Classification of the multipolarity of gamma radiation according to various changes in spin and parity.

$\Delta\pi$ \ ΔI	1	2	3	4
Yes	E1	M2	E3	M4
No	M1	E2	M3	E4

The gamma decay transition probability, $T(\lambda)$, is given by[14]

$$T(\lambda) = \frac{8\pi\,(\lambda + 1)}{\lambda[(2\lambda + 1)!!]^2}\ \frac{1}{\hbar}\ \left(\frac{\omega}{c}\right)^{2\lambda+1} B(\lambda) \tag{2.8}$$

where λ is the multipolarity, $\hbar\omega$ is the γ-ray energy and $B(\lambda)$ is the reduced transition probability. $B(\lambda)$ is given by

$$B(\lambda) = \frac{1}{2I_i + 1}\left|\langle \Gamma_f\ I_f\ \|M_\lambda\|\ \Gamma_i\ I_i\rangle\right|^2 \tag{2.9}$$

where I_i and I_f are the spins of the initial and final states, respectively, Γ_i and Γ_f are all other quantum numbers of the initial and final states, respectively, and M_λ is the appropriate multipole operator. Because of lack of detailed knowledge of the state functions, $B(\lambda)$ cannot be accurately calculated. However, γ-ray transition probabilities can be roughly estimated by using the derived wave functions of any nuclear model. Transition probabilities calculated for a single proton in a three-dimensional square-well potential are plotted in Fig. 2.[15] These curves are of value in the determination of ΔI for any observed transition. Parity changes must be determined by other means, e.g., by measurement of internal conversion coefficients[16] or by directional polarization-correlation measurements.[17]

In nuclei describable by the collective model, $B(\lambda)$ can be reduced to the product of two quantities, one being a geometric factor only and the other being a factor dependent upon the intrinsic state functions only. It is therefore possible to find the ratio of the $B(\lambda)$'s for the transitions from the state $|\Gamma_i\ I_i\ K_i\rangle$ to any two of the various possible final states in a rotational band K_f. The ratio is

$$\frac{B(\lambda : I_i \longrightarrow I_{f'})}{B(\lambda : I_i \longrightarrow I_f)} = \frac{(I_i\ \lambda\ K_i\ (K_f - K_i) \mid I_{f'}\ K_f)^2}{(I_i\ \lambda\ K_i\ (K_f - K_i) \mid I_f\ K_f)^2} \qquad (2.10)$$

It is thus possible to calculate the relative transition probabilities for the transitions from any state to the members of a rotational band.

2.5 Nuclear Isomerism. All states of a given nuclide are, by definition, isomeric states of the nuclide. In the field of nuclear spectroscopy, the usage has been modified to include only those states having measurable lifetimes. From Fig. 2 it is seen that transitions of life-time greater than one second involve a large spin change between initial and final states. It is therefore

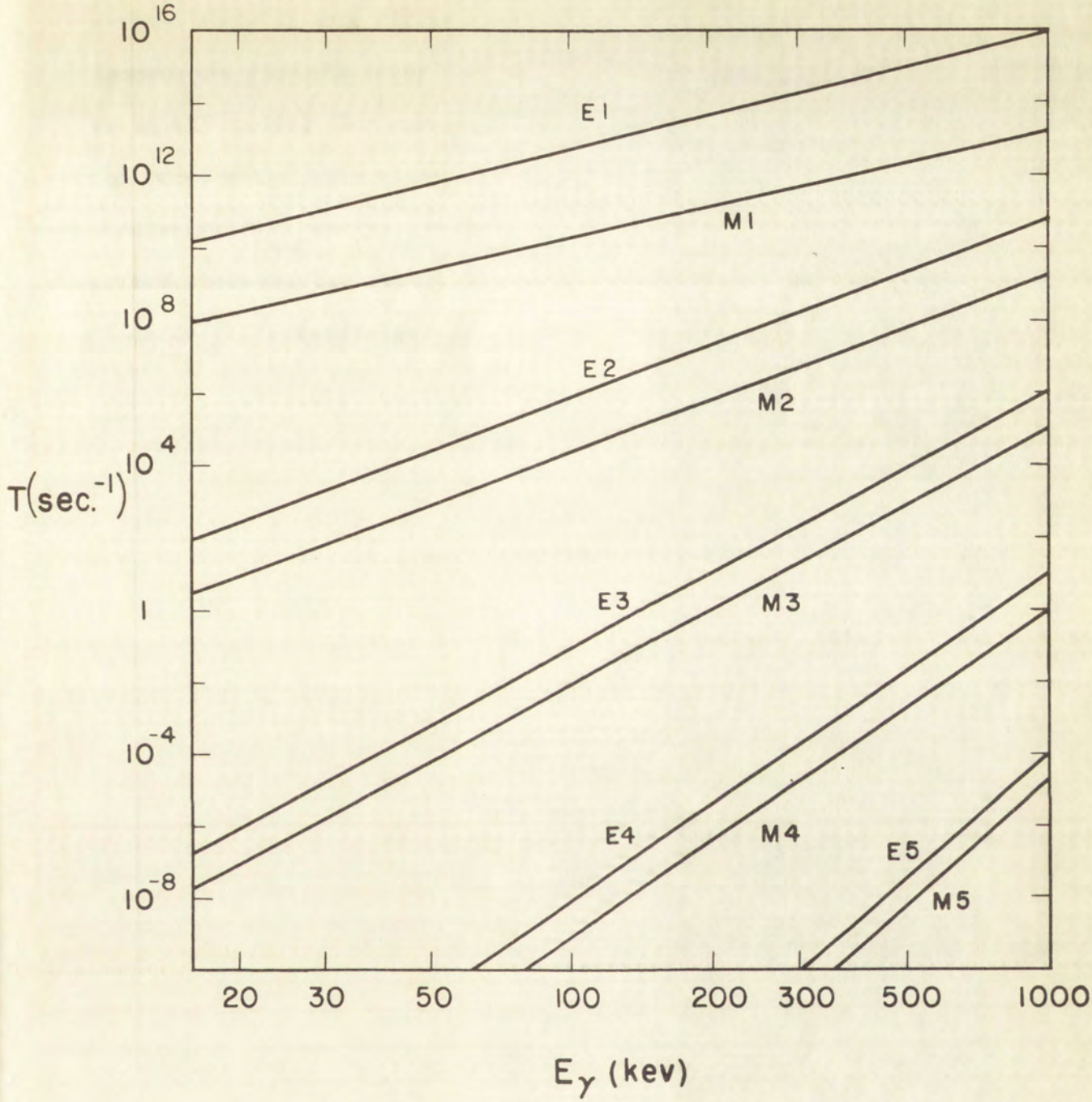

Fig. 2. Gamma-decay transition probability, T, for a single proton as a function of γ-ray energy for various multipolarities, calculated using shell-model wave functions.

expected that in odd-A nuclides, isomers will occur when the spin of the first excited state is very different from that of the ground state. Known long-lived isomers are found to occur[18] in "islands" rather than to be uniformly distributed among all nuclei. For example, a group of such isomers are known to occur in the odd-A nuclei with either N or Z between 38 and 50. In this region the shell-model $g_{9/2}$ and $p_{1/2}$ states are adjacent, one being the orbital of the ground state and the other of a low-lying excited state. All of the other "islands" of isomerism have similar shell-model explanations.

CHAPTER III

EXPERIMENTAL EQUIPMENT

3.1 The Scintillation Spectrometer. All of the γ-ray experiments reported here were conducted with a NaI(Tl) scintillation spectrometer. A brief look at the principal advantages of this type of spectrometer will reveal the power of scintillation techniques and the reasons for using this method in the present study:

(1) NaI(Tl) scintillation spectra are easy to interpret; in general, each of the observed spectral peaks (or "lines") represents a different γ ray. Although the inherent resolution is relatively poor (~8% at 0.6 Mev), the energies of resolved lines can be assigned with a standard deviation of approximately 1/2%.

(2) NaI(Tl) spectrometers have very high detection efficiencies. The efficiency of the spectrometer used in the present experiments varied from 10% to 1% as a function of energy (see Fig. 3). Although the energies of γ rays are measurable to much greater precision by bent crystal spectrometers, by using external converter techniques with electron spectrometers, and by the measurement of the energy of internal-conversion electrons, these methods have extremely low efficiency so that, in general, very intense sources are needed. The efficiency of a bent crystal spectrometer is of the order of 10^5 less than that of the scintillation spectrometer. External converter techniques are applicable only to isolated studies of extremely intense low-energy radiation. Measurement of transition energies by internal-conversion electron studies is limited to those cases in which there are sufficient numbers of conversion electrons as to be measurable when superimposed on the beta continuum.

(3) Coincidence measurements between γ rays can in principle be made with any equipment capable of detection of γ rays. In practice, however, only

scintillation spectrometers adequately meet the necessary requirements: high detection efficiency, very fast pulse rise time, and the capability of energy resolution.

(4) Present-day scintillation spectrometer instrumentation permits counting rates as high as 10,000 counts per second without noticeable spectral distortion. This makes possible the accumulation of statistically meaningful data in relatively short counting times, a feature which is particularly valuable in coincidence measurements.

(5) When a scintillation spectrometer is used in conjunction with a 100-channel analyzer, spectral data on all parts of a large energy region can be recorded simultaneously. This results in a tremendous savings of time and also eliminates the usual time corrections introduced by source decay.

In conclusion, except for precision energy measurements, the scintillator technique is infinitely superior to other present-day methods of studying γ-ray spectra. Excluding half-life measurements, none of the information reported in this paper could possibly have been obtained by other techniques.

Since the scintillation technique is the main experimental method used in this research a short discussion of scintillator theory seems appropriate. The fundamental principle involved in the scintillation detector is the conversion of the energy of nuclear radiation into light flashes which in turn produce current pulses in a photomultiplier tube. These current pulses are directly proportional to the amount of energy deposited in the crystal. From analysis of the frequency distribution of pulse heights, energies and intensities of γ rays can be determined.

The performance of the spectrometer is governed principally by the choice of scintillating material and by the physical dimensions and technique used to mount the scintillator on the photomultiplier tube. There are many materials known which scintillate. Because of the great variation in physical

properties and scintillation characteristics of phosphors a wide variety of materials are used, each in the application to which it is best suited. The most commonly used scintillators and their principle pertinent characteristics are presented in Table III.

TABLE III. Characteristics of commonly used scintillators.

Material	Relative light output	Decay constant x 10^{-8} sec	Density g/cm^3	Applications
Anthracene	1.0	3.0	1.25	α,β,γ,Fast n
Stilbene	0.65	0.8	1.16	"
Plastic phosphor	0.6	0.3	1.03	"
NaI(Tl)	2.0	25	3.67	γ
$CaWO_4$	1.0	300	6.06	γ
CsI	0.7	110	4.51	γ
LiI(Eu)	3.0	20	4.06	slow n

Gamma rays interact with matter by three principal processes: Compton scattering, the photoelectric effect, and pair production.[20] Compton scattering is the elastic scattering of γ rays from atomic electrons and is the dominant mode of interaction in the neighborhood of 1 Mev. Part of the energy of the incident photon is transferred to the electron; the balance of the energy is carried away by the scattered photon. The electron is normally stopped in the scintillator, while the scattered photon may either itself be detected or leave the crystal.

Detection by the photoelectric effect involves transfer of the entire photon energy to a bound electron. Part of the energy is used to overcome the

electron binding energy, and the rest of the energy appears as electron kinetic energy. The atomic-shell vacancy created by the ejection of an electron gives rise to an electron "cascade", with which is associated an emission of x radiation whose total energy is equal to the binding energy of the original electron. Except in certain events which occur very near a crystal edge, the electron and x-ray energies will be trapped in the phosphor, giving a light pulse whose intensity is directly proportional to the incident photon energy. The photoelectric effect is the predominant type of interaction at photon energies below 0.5 Mev.

In pair production, a photon in the field of a nucleus disappears with the simultaneous creation of an electron-positron pair whose total kinetic energy is the photon kinetic energy minus the mass energy of the two created particles. Thus, the threshold energy for pair-production is $2m_oc^2$ (1.022 Mev). Since all γ rays studied in the present experiments have energies <1 Mev, no further discussion of the pair-production interaction will be presented.

The ideal scintillator would have the property that incident quanta of the same energy would always produce a light pulse of the same amplitude. Because this is a characteristic of detection by the photoelectric effect, it is advantageous to choose a scintillator with high photoelectric cross section relative to the Compton and pair-production cross sections. No single formula for the pair production and photoelectric cross sections has been developed which is accurate over the extremes of photon energy and detector atomic weight. Examination of the piecewise-accurate formulae show that for a fixed photon energy the cross section per atom for the photoelectric effect, Compton scattering, and pair production vary as Z^5, Z, and Z^2, respectively. Therefore, the obvious choice of scintillator for γ-ray detection is one whose principle constituent is of high Z.

A second major factor in the selection of a scintillation medium is the luminous efficiency, i.e., the fraction of the incident photon energy emitted by the scintillator as light. The importance of the luminous efficiency lies in its influence on the energy resolution of the spectrometer. To first order the resolution is inversely proportional to the square root of the average number of electrons per pulse incident on the first dynode of the photomultiplier tube. The number of electrons which strike the first dynode is the product of the incident photon energy, the luminous efficiency, the optical efficiency, the photocathode efficiency, and the electron collection efficiency. It is therefore obvious that high luminous efficiency is desirable.

The most satisfactory scintillator for γ-ray spectroscopy which has yet been developed is thallium-activated sodium iodide, NaI(Tl). Its desirable properties include a relatively high Z, high luminous efficiency, and a relatively short decay constant.

The response of a scintillation spectrometer to γ rays is in general quite complex and for that reason will be briefly discussed before consideration is given to crystal dimensions and mounting. Figure 4 shows the pulse-height spectrum observed when 0.662-Mev quanta are incident on a 2 x 2-in. NaI(Tl) crystal. Note the two gross features, the sharply peaked distribution resulting primarily from detection by the photoelectric effect and the continuous distribution resulting from detection by the Compton effect.

The Compton distribution results from those Compton events in which the scattered quanta have escaped from the scintillator. A scattered quantum may instead deposit its energy in the scintillator through a photoelectric event, in which case the multiply-generated light pulse will have the same energy content as the pulse which would have occurred if the incident primary quantum had itself been detected by the photoelectric process.

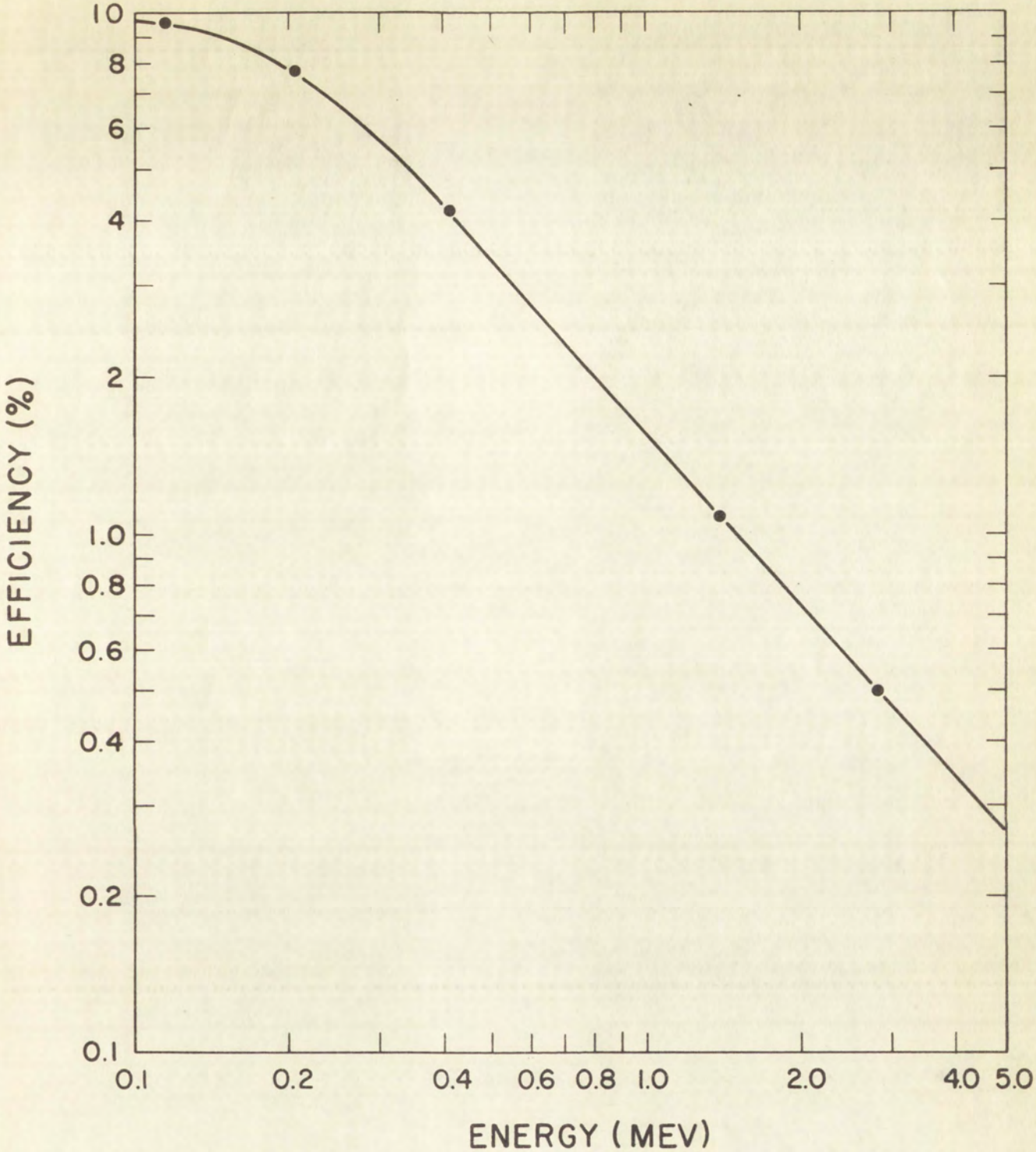

Fig. 3. Photopeak efficiency of a 2 x 2-inch NaI(Tl) scintillation detector as a function of energy. Efficiency of the scintillation spectrometer for the detection in the photopeak of γ rays of various energies.

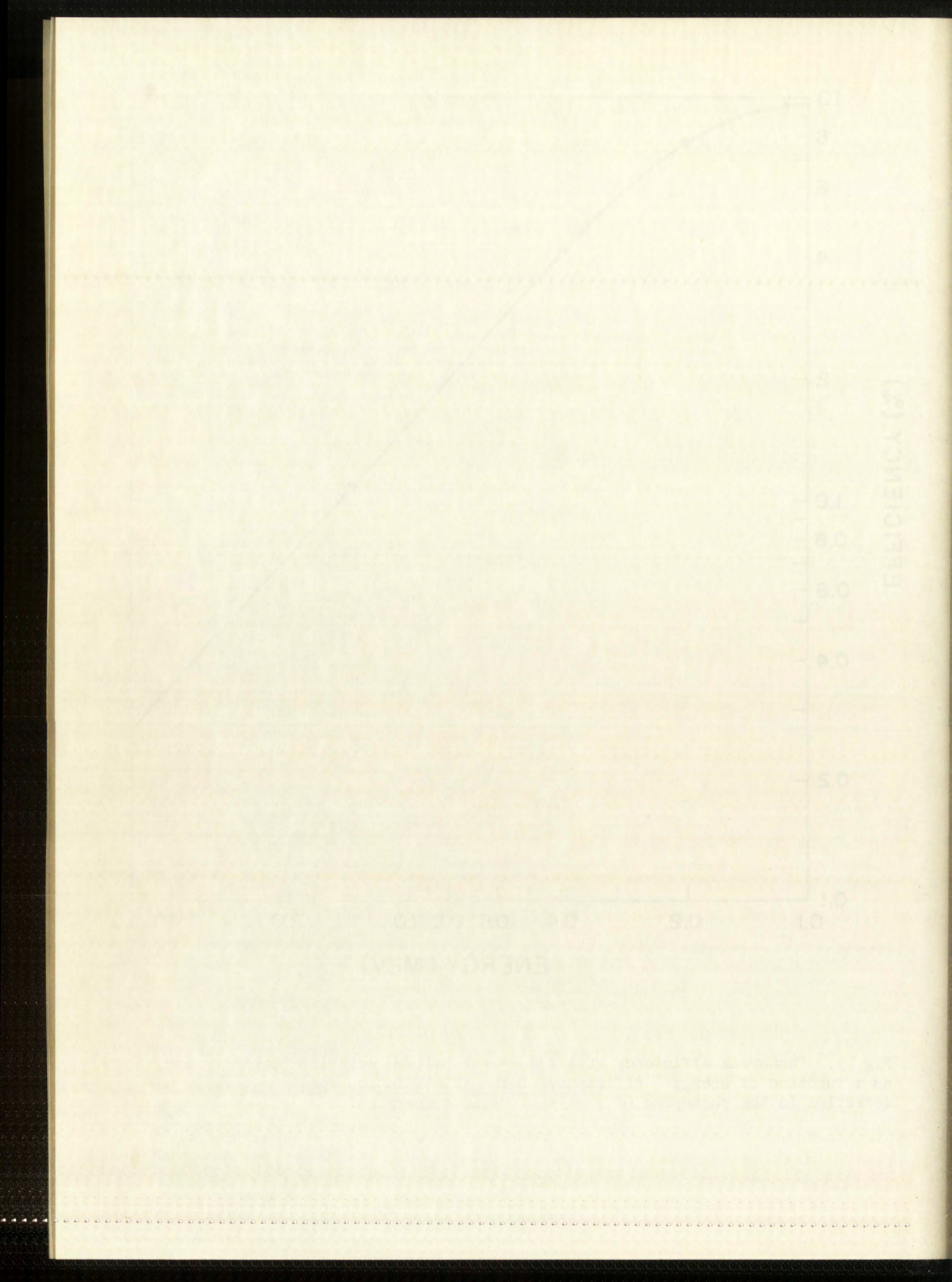

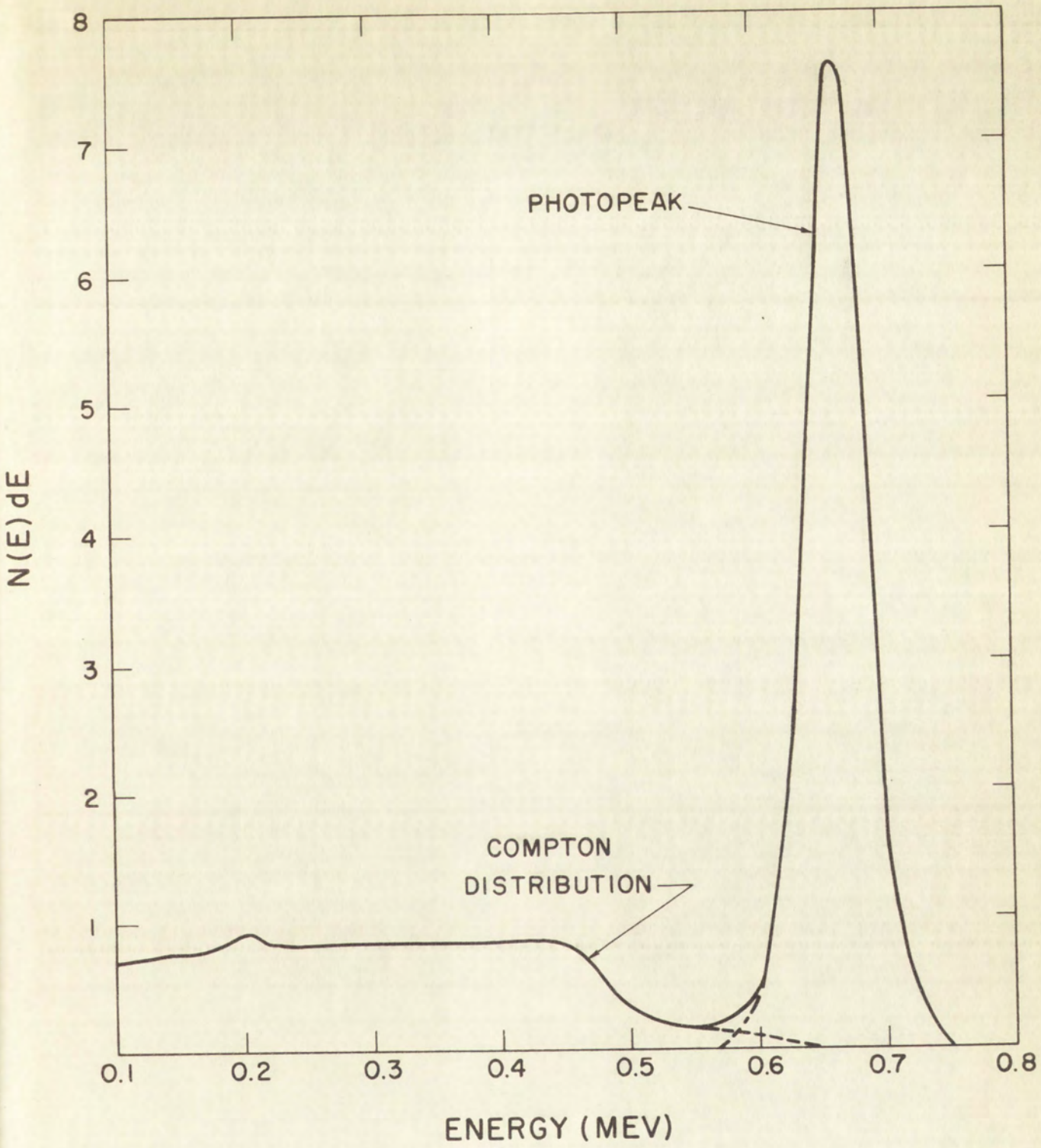

Fig. 4. Response of the scintillation spectrometer to γ rays of energy 662 kev (Cs^{137}).

Because the probability of multiple detection increases rapidly with crystal dimensions and because of the rapidly increasing photon mean free path with increasing energy, it is evident that for energetic γ rays a large crystal is desirable. The NaI(Tl) crystals used in these experiments were cylinders 2 inches in diameter by 2 inches high. These crystals were mounted on RCA-6342 photomultiplier tubes, using the technique developed by P. R. Bell.[19]

The voltage pulse at the anode of the photomultiplier tube is normally much less than 1 volt so it must be amplified. The amplifiers used in this work were 1 μsec delay-line-clipped nonoverloading amplifiers with continuously adjustable gain control. They are able to withstand pulse-amplitude "overload" factors of 100 at counting rates of 10^4 counts per second with no discernable base-line shift. These amplifiers can deliver output pulses with amplitudes as high as 120 volts; however, they are linear (within 1%) only in the pulse-height range of 10 to 95 volts. The output pulses of a given amplifier were either analyzed with a 100-channel differential pulse-height analyzer, or used to trigger the coincidence circuit (or both).

The 100-channel pulse-height analyzer used is of the pulse-height-to-time conversion type in which computer-type magnetic memory cores are used as storage elements. The average time required to analyze and store a pulse is 10 μsec. Because this dead-time introduces no spectral distortion, the analyzer can be used at the maximum counting rate at which the rest of the electronic system performs satisfactorily. The analyzer can be employed either to analyze all pulses received or to analyze only those pulses coincident in time with pulses from another detector. The data can be presented in any combination of four forms: a visual display, a printed tape, a punched tape for direct transfer of data to electronic computers, and an automatically plotted histogram of counts per channel versus channel number.

The coincidence circuit employed has in each input channel a variable lower and upper bound control to allow coincidence measurements to be performed between selected portions of the pulse-height distribution. Incorporated in the circuit is a variable resolving time of 0.4, 0.7, 1.0, 1.3, and 1.6 μsec. Also included in each channel are variable time delays of 0.1, 0.3, 0.5, and 0.8 μsec which are needed to compensate for timing differences in the two detection systems. This is necessary when the two scintillators used have different decay constants.

A picture of the electronic equipment used in these experiments is shown in Fig. 5, and a block diagram of this equipment is shown in Fig. 6.

3.2 The Methane Flow Proportional Counter. During the course of this work it was necessary to measure beta disintegration rates. For this purpose a detector was required which had high detection efficiency for β rays and low detection efficiency for γ rays, and in addition had excellent long-time stability. The detector used was a conventional methane-flow proportional counter of the type used by Group J-11, the radiochemical group of this Laboratory.

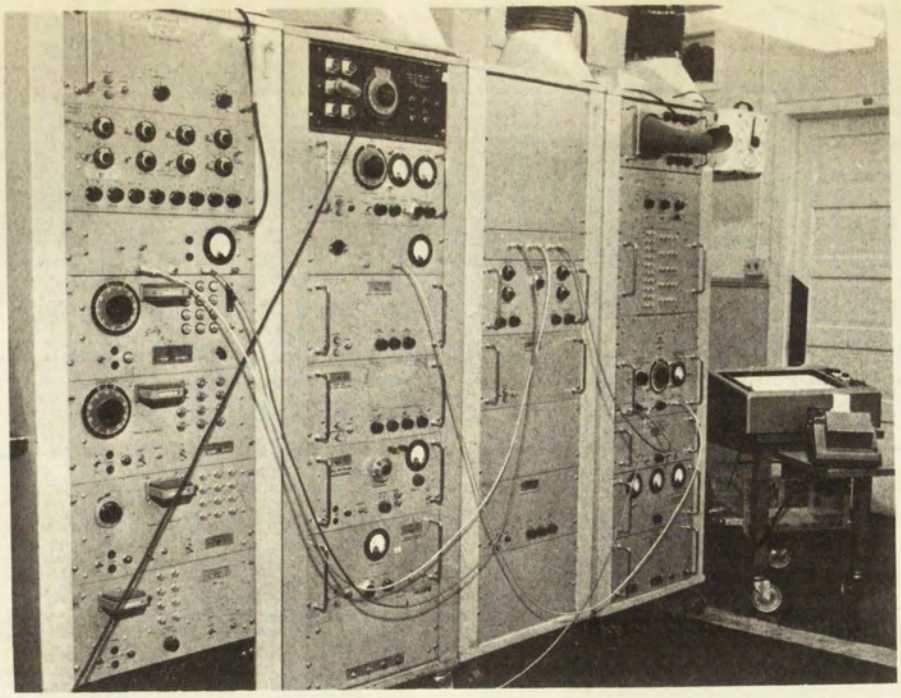

(a)

LINEAR AMPLIFIER	PHOTO-TUBE PWR SUPPLY		100 CHANNEL ANALYZER
4-CHANNEL COINCIDENCE CIRCUIT	SYSTEM GAIN STABILIZER		
SCALER	LINEAR AMPLIFIER	2-CHANNEL COINCIDENCE CIRCUIT	
SCALER	DELAY LINE AND DRIVER	COINCIDENCE PWR SUPPLY	
SCALER	PULSER		
COINCIDENCE PWR SUPPLY WITH SCALER	PHOTO-TUBE PWR SUPPLY	LINEAR AMPLIFIER	
VOLTAGE REGULATOR	VOLTAGE REGULATOR		

PLOTTER AND PRINT-OUT

(b)

Fig. 5. (a) Electronic equipment for the scintillation spectrometer. (b) Legend.

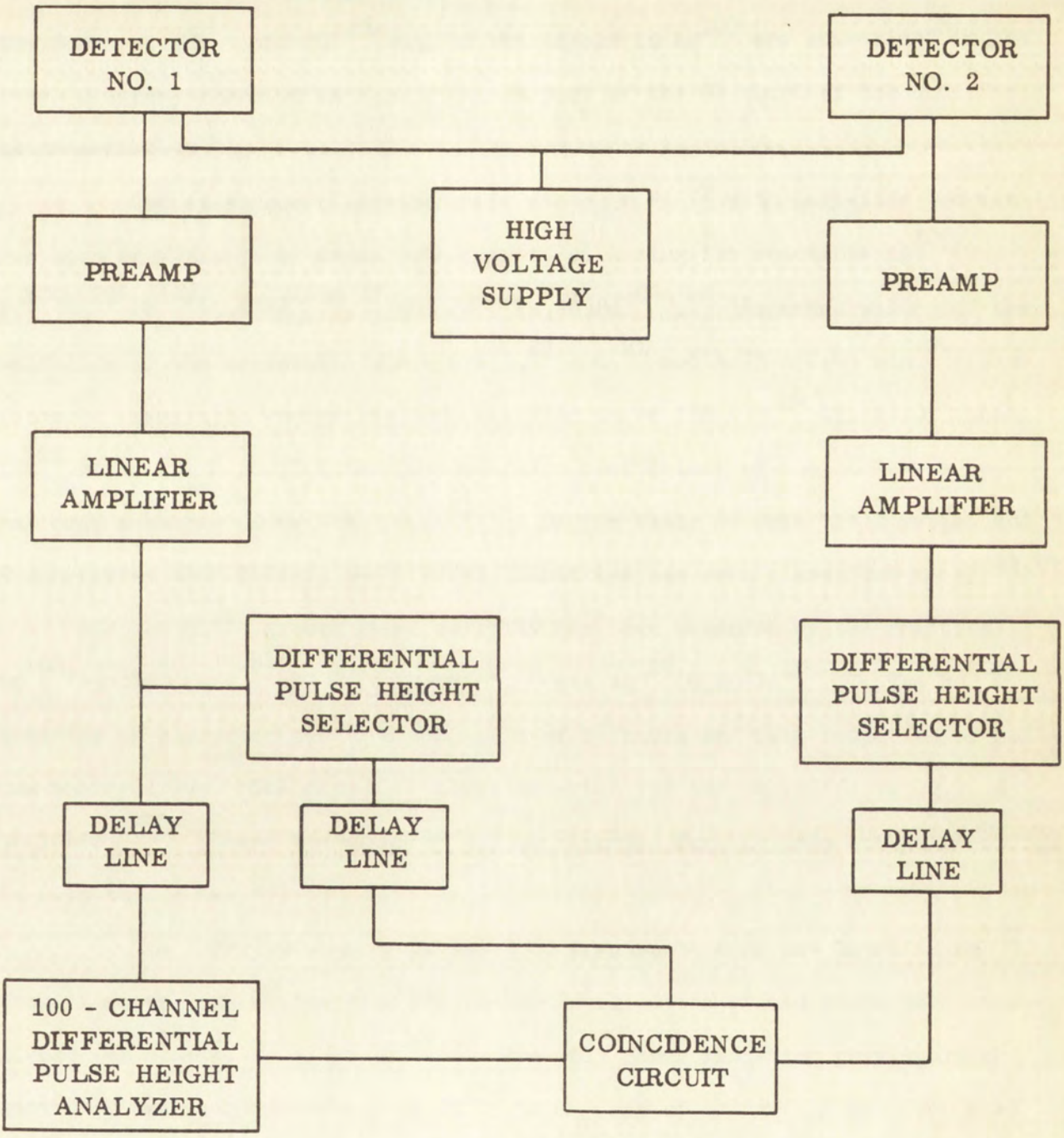

Fig. 6. Block diagram of the electronic equipment.

CHAPTER IV

EXPERIMENTAL RESULTS

4.1 Previous Investigations. The previously published data pertinent to the decay of Pd^{109} and Pd^{109m} and to the levels in Ag^{109} are summarized in the level diagram presented as Fig. 7.[6,7] A part of the GE chart of the nuclides is presented in Fig. 8 to assist in the arguments to follow.

The existence of a metastable state in Pd^{109} with half-life 4.8 min has been established by cross bombardment, utilizing the reactions $Ag^{109}(n,p)Pd^{109m}$,[21] $Pd^{108}(n,\gamma)Pd^{109m}$,[22] and $Pd^{110}(n,2n)Pd^{109m}$.[22] Reported values of the half-life of the metastable state are 5,[23] 4.8,[21] and 4.75 ± 0.05 min.[24] The isomeric transition energy has been reported to be 188 ± 5,[24] 173 ± 10,[23] and 160[21] kev. The K shell internal-conversion coefficient of the 188-kev γ ray has been measured to be 0.6 ± 0.1.[21,24] On the basis of both the lifetime and K conversion coefficient, the 188-kev transition has been classified as E3.[21,24]

The Pd^{109} ground state activity has been produced by the reactions $Pd^{108}(n,\gamma)Pd^{109}$,[25-27] $Pd^{110}(n,2n)Pd^{109}$,[26] and $Ag^{109}(d,2p)Pd^{109}$.[28] The Pd^{109} activity is characterized by a half-life of 14 hours and beta radiation of maximum energy 1 Mev. The range of values reported for the half-life is 12.7 to 14.1 hrs,[26,29-32] and the range of values reported for the beta end-point energy is 0.95 to 1.1 Mev.[33-35]

The 1-Mev beta group is known to populate the 88 kev level in Ag^{109}. Studies of the transition from the 88 kev level to the ground state have established its multipolarity as E3.[33,36] The only other radiation previously observed to accompany the decay of Pd^{109} is a γ ray of energy 312 kev, reported to have an intensity of 7×10^{-4} per disintegration.[36]

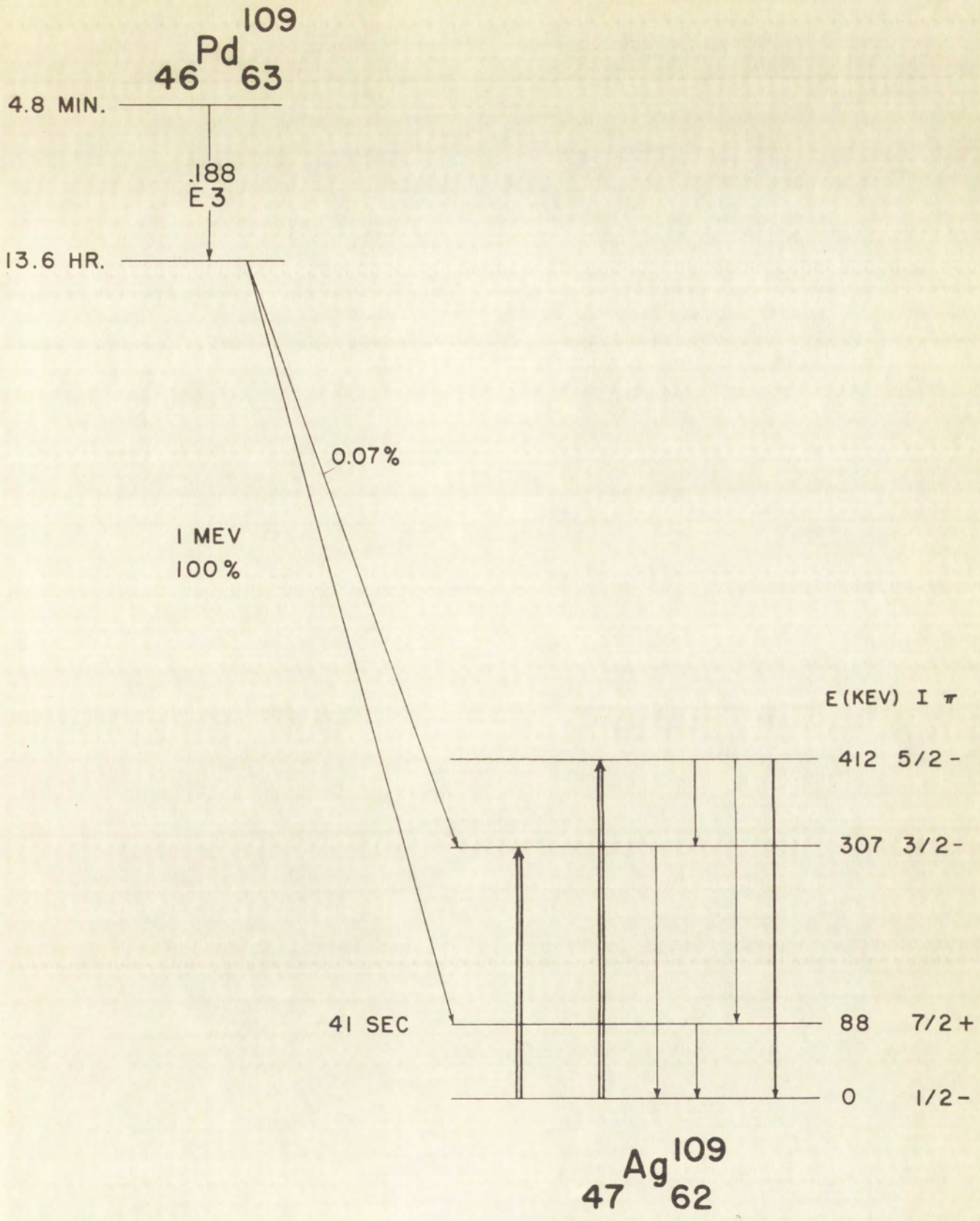

Fig. 7. Schematic summary of the previously published data on the decay of Pd^{109m} and Pd^{109}.

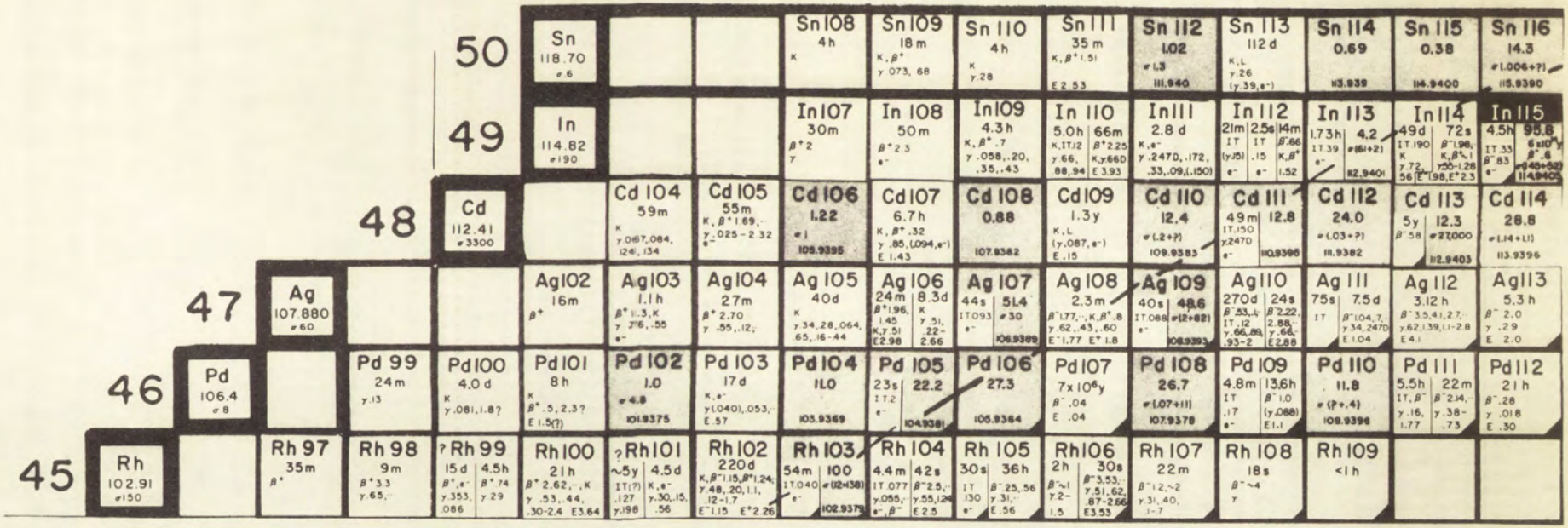

Fig. 8. A portion of the General Electric Chart of the Nuclides.

The spin of the Ag^{109} ground state has been measured to be $I = 1/2$.[37,38] Coulomb excitation studies[39-43] have shown the existence of levels in Ag^{109} at 307 and 412 kev, and, by analysis of the angular distribution of the de-excitation γ rays with respect to the incident proton beam, have established the spin sequence and multipolarity of the 412- and 307-kev γ transitions to be 5/2 (E2) 1/2, and 3/2 (M1 + E2) 1/2, respectively.[39] The lifetimes of the 307- and 412-kev transitions,[39] as inferred from the measured Coulomb excitation cross sections, are about 25 times less than the calculated values for single particle transitions, thus inferring that these transitions are of a collective nature. These experiments imply the existence of a ground-state rotational band, with spin sequence 1/2, 3/2, 5/2. Coulomb excitation studies have also shown the existence of 1/2, 3/2, 5/2 ground-state rotational bands in the nuclides Ag^{107} and Rh^{103}.[5-7]

4.2 Source Preparation. All sources used to study the decay of Pd^{109} were prepared by thermal neutron irradiation of ~10-mg samples of $Pd(NO_3)_2$. Activities other than the desired Pd^{109} activity were expected and observed. These activities are of two types: other palladium activities, and activities induced in impurities present in the source material.

As can be seen by reference to Fig. 8, palladium occurs in nature as a mixture of six stable isotopes. Thermal neutron irradiation of natural palladium will produce, in addition to the desired Pd^{109}, the radioactive isotopes Pd^{103}, Pd^{105m}, Pd^{107}, Pd^{109m}, Pd^{111m}, and Pd^{111}. It is evident from half-life considerations that the Pd^{105m} and Pd^{109m} activities will soon decay to negligible intensity, and that the amount of Pd^{107} activity produced is insignificant. The ratio of initial activities of Pd^{109} to Pd^{103}, calculated from the isotopic abundances and (n,γ) cross sections of Pd^{108} and Pd^{102}, is 1.8×10^3. This ratio is sufficiently favorable that in only one experiment were the known

radiations of Pd^{103} detected. The radiations of Pd^{111m} and Pd^{111} were initially much less intense than those of Pd^{109}, and were effectively eliminated by allowing the source material to decay for 40 hours before chemical purification and counting.

The principal activities induced in impurities present in the source material were identified by their radiations to be Na^{24}, Ag^{108}, Au^{198}, and Ir^{194}. These activities were effectively removed by the following purification procedure, which is a simplified version of a procedure given in reference 44:

Step 1. Dissolve the source material in conc HCl. Add Ag and Ir carriers and boil for 5 minutes to promote exchange between contaminants and carriers.

Step 2. Make solution 0.4 molar in HCl and centrifuge. Transfer the supernate to a clean centrifuge tube.

Step 3. Add 5 ml of 1% solution of sodium dimethylglyoxime in 95% ethanol and centrifuge. Discard the supernate.

Step 4. Dissolve by heating the precipitate in 1 ml conc HNO_3 containing a few drops conc HCl. Add Ag and Ir carriers. Dilute with 10 ml H_2O and centrifuge. Transfer the supernate to a clean centrifuge tube.

Step 5. Add 5 ml of 1% solution of sodium dimethylglyoxime in 95% ethanol and filter. Wash with H_2O and ethanol.

The above procedure was found to give a decontamination factor in excess of 10^4 for each of the known contaminants.

The sources used to study the decay of Pd^{109m} were prepared by thermal neutron irradiation of PdO in which the palladium was electromagnetically enriched to 84% (by weight) in isotope Pd^{108}. The sources were encapsulated in polyethylene to prevent loss or contamination of the costly source material.

The reason for using electromagnetically enriched Pd^{108} as the source material was to obtain the maximum ratio of activities of Pd^{109m} to Pd^{111} and Pd^{105m}. The activities of Pd^{105m} and Pd^{111} were, in fact, never observed. Another advantage realized from the choice of source material was that the spectroscopic-grade purity made chemical purification unnecessary.

4.3 Half-Life Measurements. The half-life of Pd^{109} was determined by measuring the time dependence of the disintegration rate of a Pd^{109} source. The radioactive decay law relating the time t, the disintegration rate A, and the decay probability per unit time, λ, is

$$A(t) = A(o)\, e^{-\lambda t}. \tag{4.1}$$

By definition, the half-life, $T_{1/2}$, is given by the relationship

$$T_{1/2}\, \lambda = \ln 2. \tag{4.2}$$

The decay data were obtained with a methane flow proportional counter. Corrections were made to the data for natural background counts and for counting-loss due to the finite resolving time of the counter. The resolving time was determined to be 6.5×10^{-6} sec. The counting-loss correction applied was determined from the following expression relating the resolving time, $\mathcal{T}$, the observed counting rate, N_o, and the true counting rate, N_t:

$$N_t\, (1 - \mathcal{T} N_o) = N_o. \tag{4.3}$$

λ was then obtained by fitting the corrected data to Eq. (4.1) by a least squares calculation. The corresponding value of $T_{1/2}$ is obtained by

substituting the value of λ into Eq. (4.2). Two determinations of the half-life were made; the values obtained were 13.482 ± 0.027 and 13.439 ± 0.013 hrs. The weighted average of these values is 13.453 ± 0.012 hrs, where the deviation quoted is purely statistical (it does not include systematic errors). A conventional semi-logarithmic plot of counting rate vs. time for one of these runs is shown in Fig. 9.

The Pd^{109m} half-life was determined in a manner fundamentally the same as that described above; however, it was necessary to analyze the data in a slightly different way. Pd^{109m} decays to Pd^{109}, which is also unstable, and as the radiations of both Pd^{109} and Pd^{109m} are detected, the equation relating disintegration rate to time is now

$$A(t) = A_1(o)\, e^{-\lambda_1 t} + A_2(o)\, e^{-\lambda_2 t}, \qquad (4.4)$$

where the subscripts refer to the two activities involved. The optimum experimental procedure is that for which the ratio of the initial counting rates of Pd^{109m} to Pd^{109} is a maximum. This was achieved by using a NaI(Tl) scintillation spectrometer to detect the 188-kev γ ray of Pd^{109m}. Some of the bremsstrahlung distribution associated with the Pd^{109} beta activity was also unavoidably detected. The only correction which needed to be applied to the data was that for natural background. The corrected data were fitted by the method of least squares to Eq. (4.4). From the value of λ obtained for Pd^{109m}, the half-life was obtained as before. Two determinations of the half-life yielded values of 4.704 ± 0.016 and 4.670 ± 0.014 min, the weighted average of which is 4.687 ± 0.011 min. One set of data is presented graphically in Fig. 10.

The half-life of Ag^{109m} was determined in the manner described for the Pd^{109m} half-life measurement. The scintillation spectrometer was set to

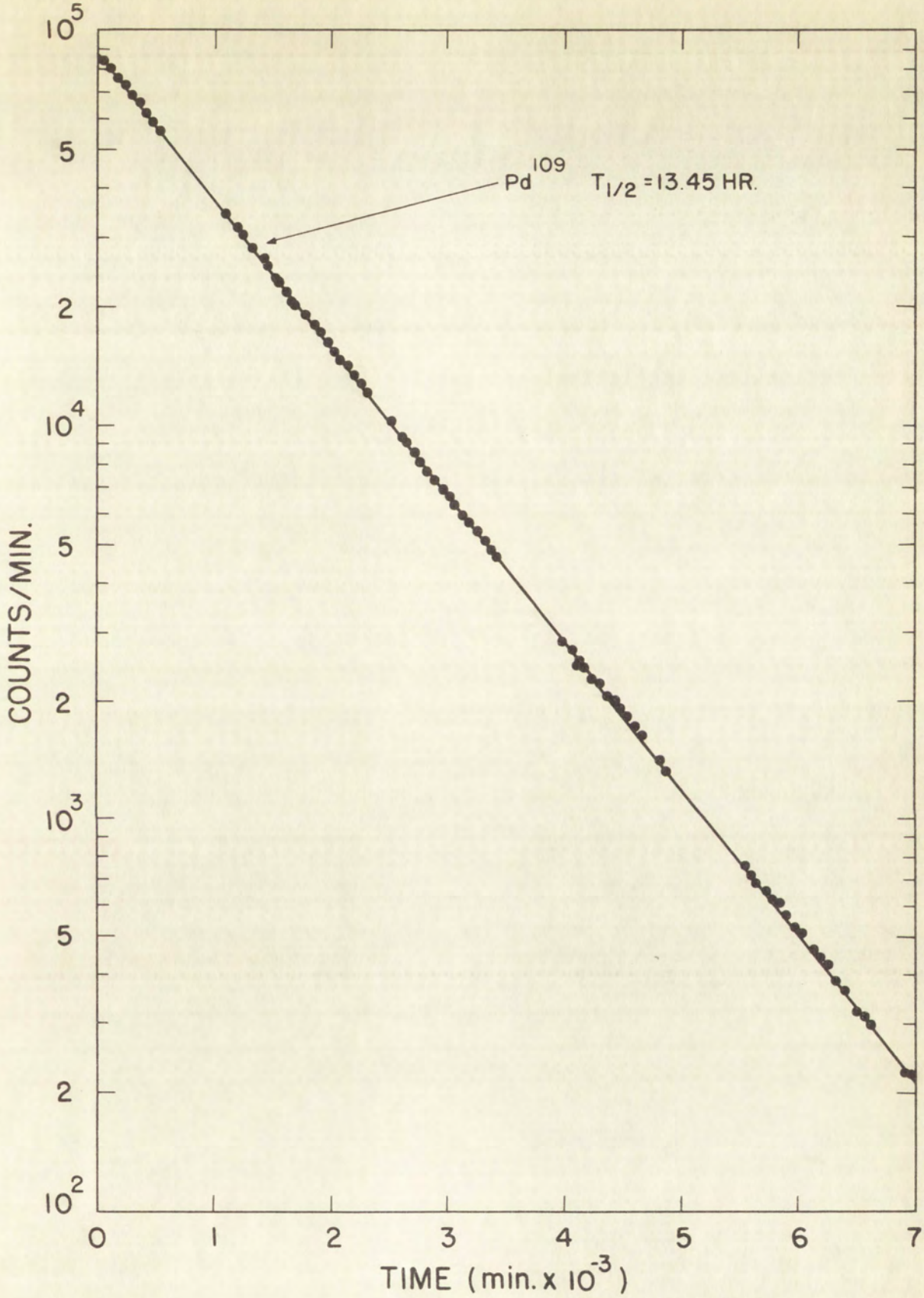

Fig. 9. Decay rate of a Pd^{109} source as a function of time.

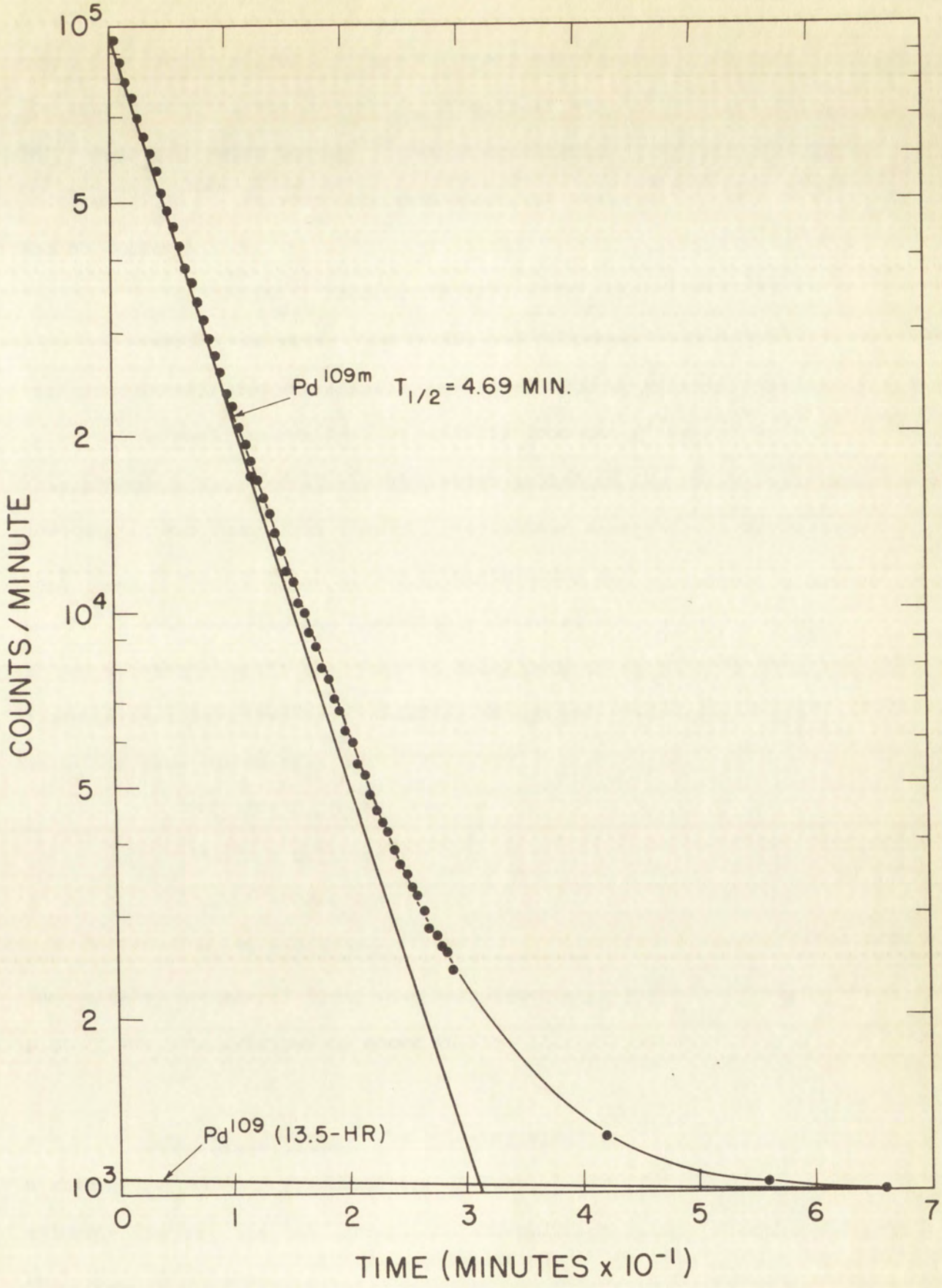

Fig. 10. Decay rate of a Pd^{109m} source as a function of time.

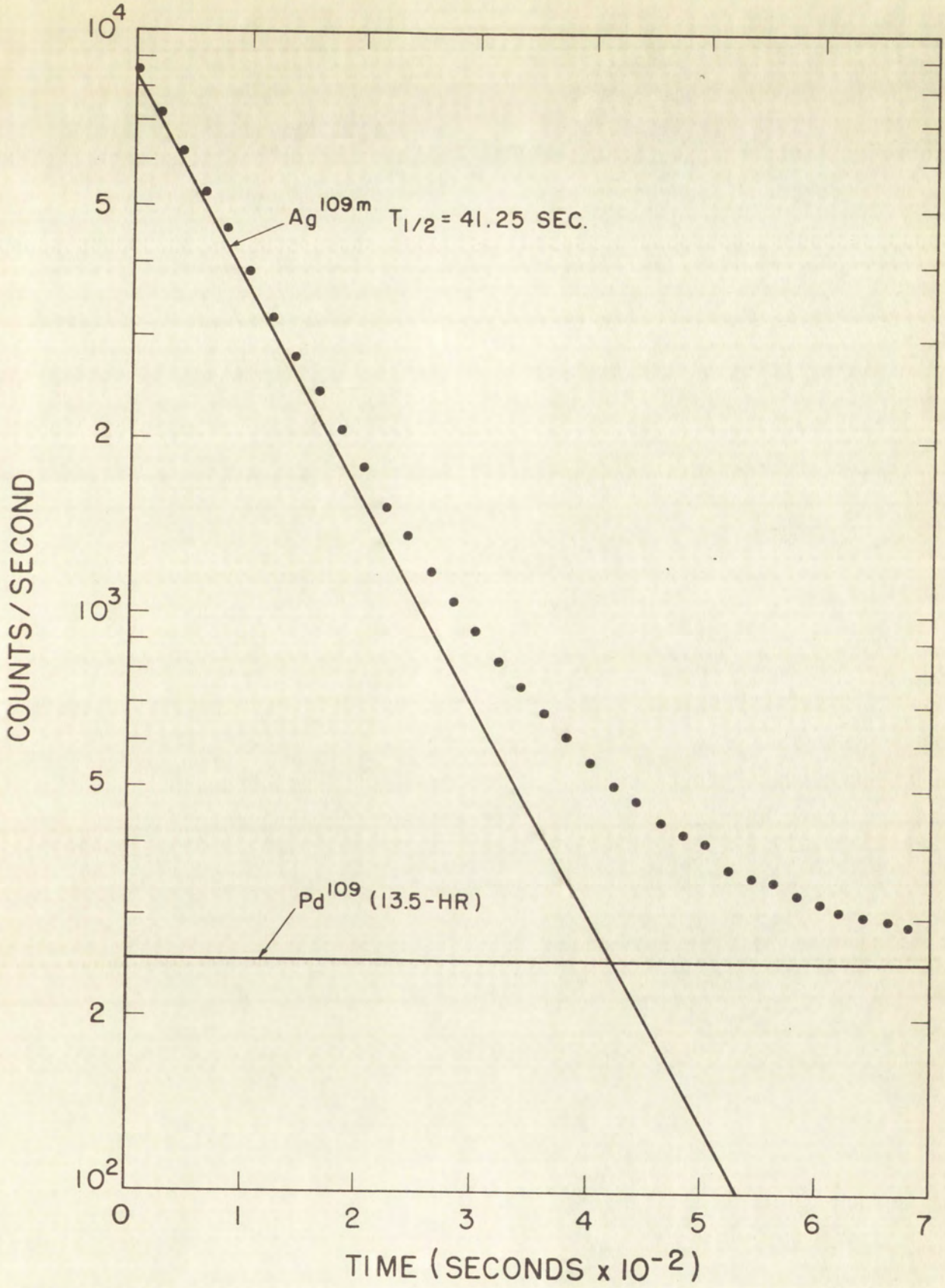

Fig. 11. Decay rate of a Ag^{109m} source as a function of time.

4.5 Gamma-Ray Experiments. The scintillation spectrum of the gamma radiation accompanying the decay of Pd^{109m} is presented in Fig. 12. These data were obtained with the NaI(Tl) scintillation spectrometer previously described. A beryllium absorber 1/8" thick was used to stop the beta rays accompanying the decay of Pd^{109}, which is always unavoidably present. The spectrum of Fig. 12 was obtained by subtracting the natural background and Pd^{109} γ-ray background from the observed data. The salient features of the Pd^{109m} spectrum are a 188 kev γ-ray photopeak and the Pd K x-ray photopeak which results from K-shell internal conversion of the 188-kev transition. A careful search was made for other possible γ rays associated with the decay of Pd^{109m}. Spectra were obtained with various thicknesses of lead absorber placed between the source and detector. No other γ-ray photopeaks were observed which could be attributed to Pd^{109m}.

The low-energy portion of the Pd^{109} γ-ray scintillation spectrum is shown in Fig. 13. Only the previously reported 88-kev γ-ray and Ag K x-ray photopeaks are observed.

The portion of the Pd^{109} photon spectrum above 200 kev is presented in Fig. 14. In this experiment a composite absorber of 0.125 in. of beryllium, 0.020 in. of lead, 0.015 in. of cadmium, and 0.005 in. of copper was placed between the source and detector. The beryllium was used to stop the beta rays, and the lead was used to preferentially absorb the very intense K x-rays and 88-kev γ rays. The purpose of the cadmium was to absorb the fluorescence radiation from the lead absorber ($\sim$72 kev), and the copper was used to absorb the cadmium fluorescence radiation.

Inspection of Fig. 14 reveals that the bulk of the observed spectrum is a photon continuum, the intensity of which decreases monotonically as a function of (increasing) energy. Superimposed on this continuum are several γ-ray photopeaks. The photon continuum is attributed to bremsstrahlung

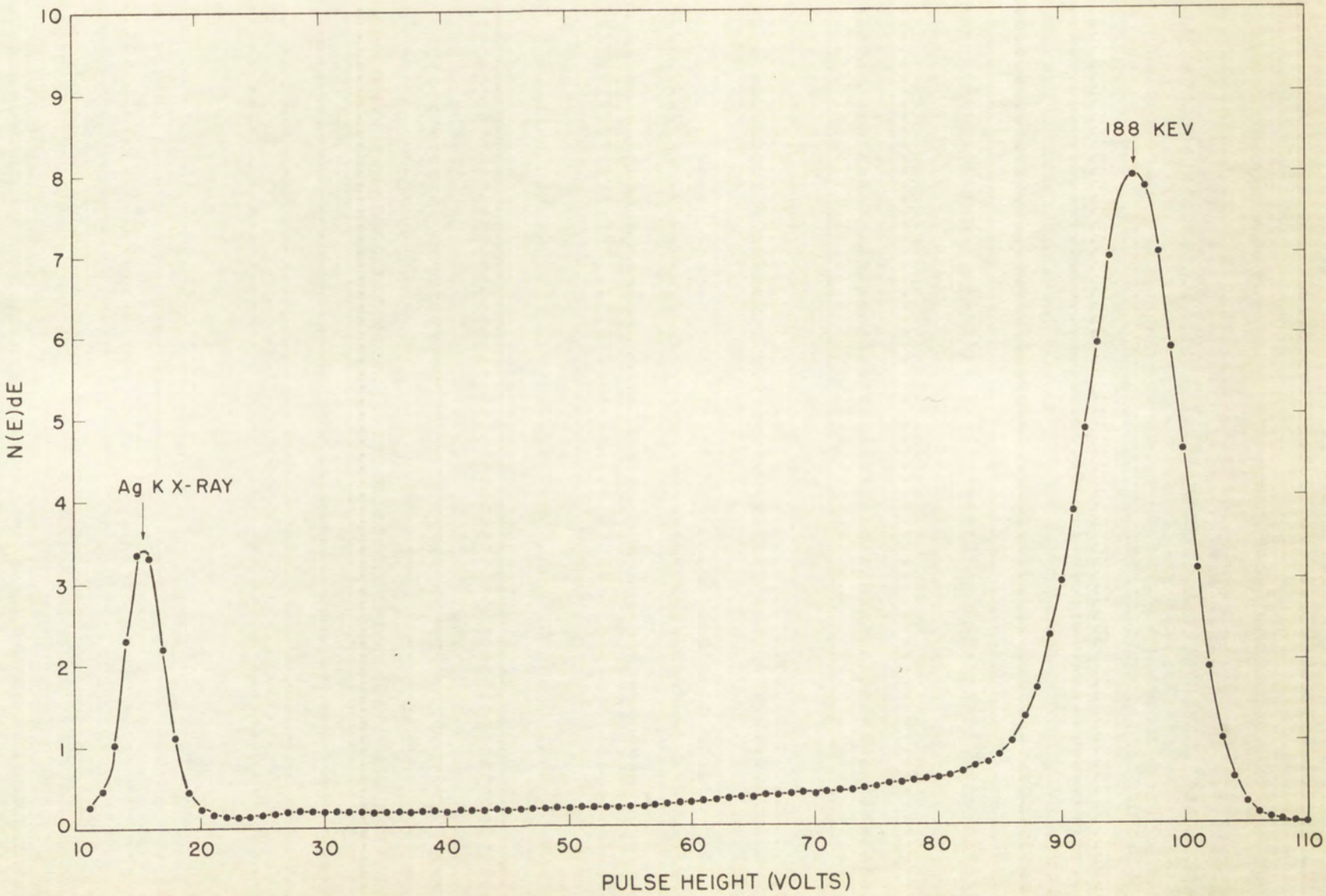

Fig. 12. Gamma-ray scintillation spectrum of Pd^{109m}.

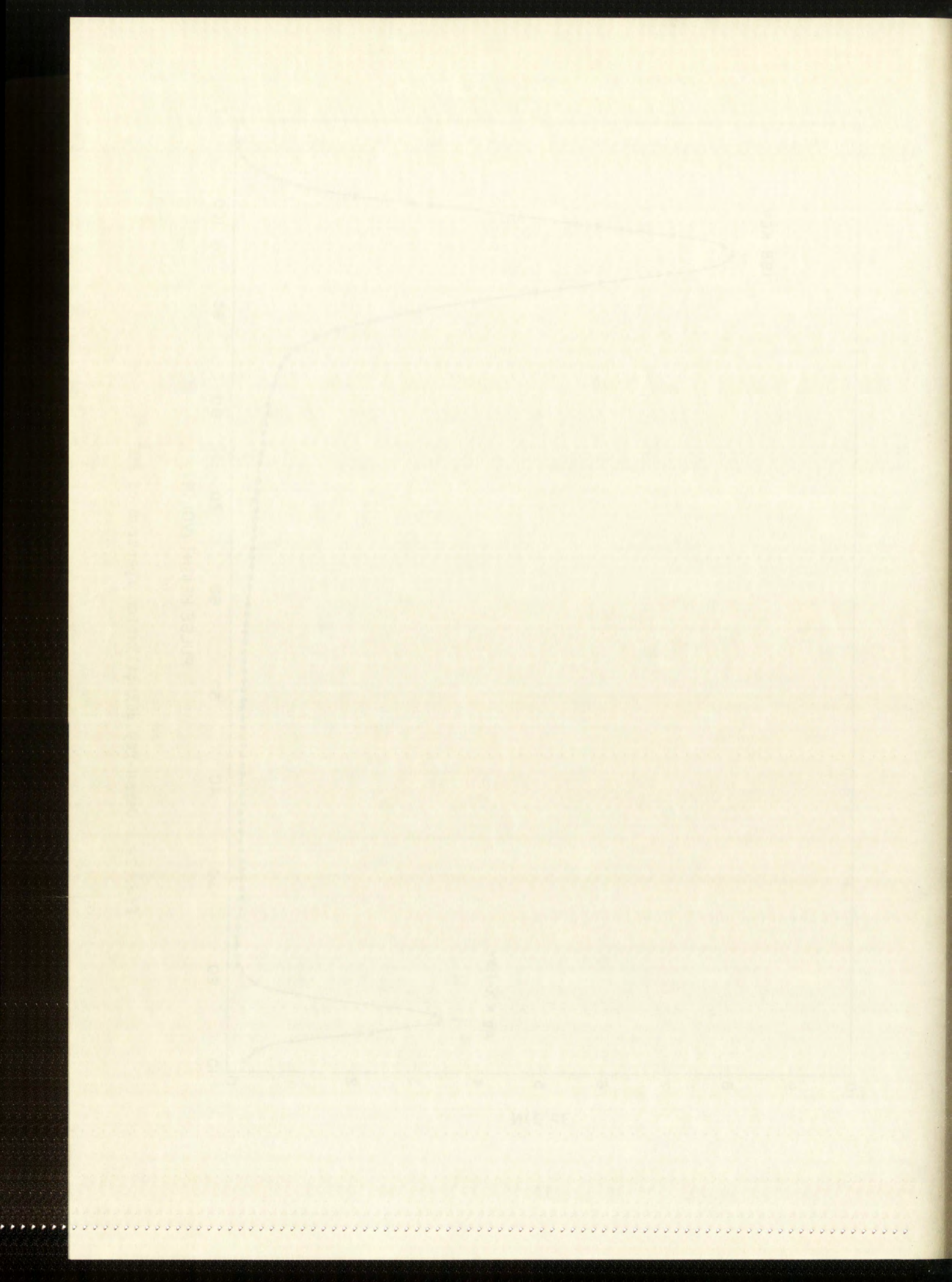

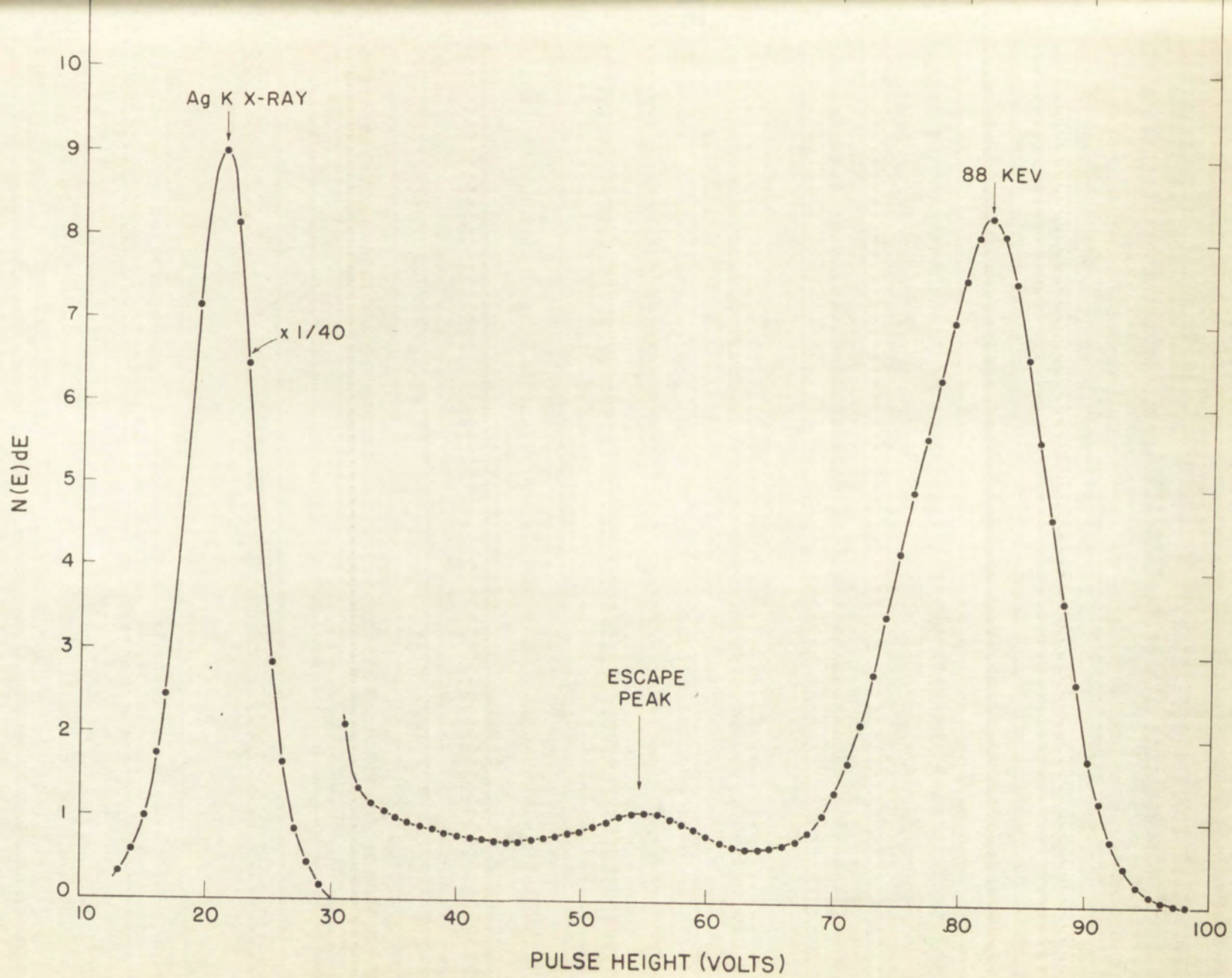

Fig. 13. Low-energy portion of the photon spectrum of Pd^{109}.

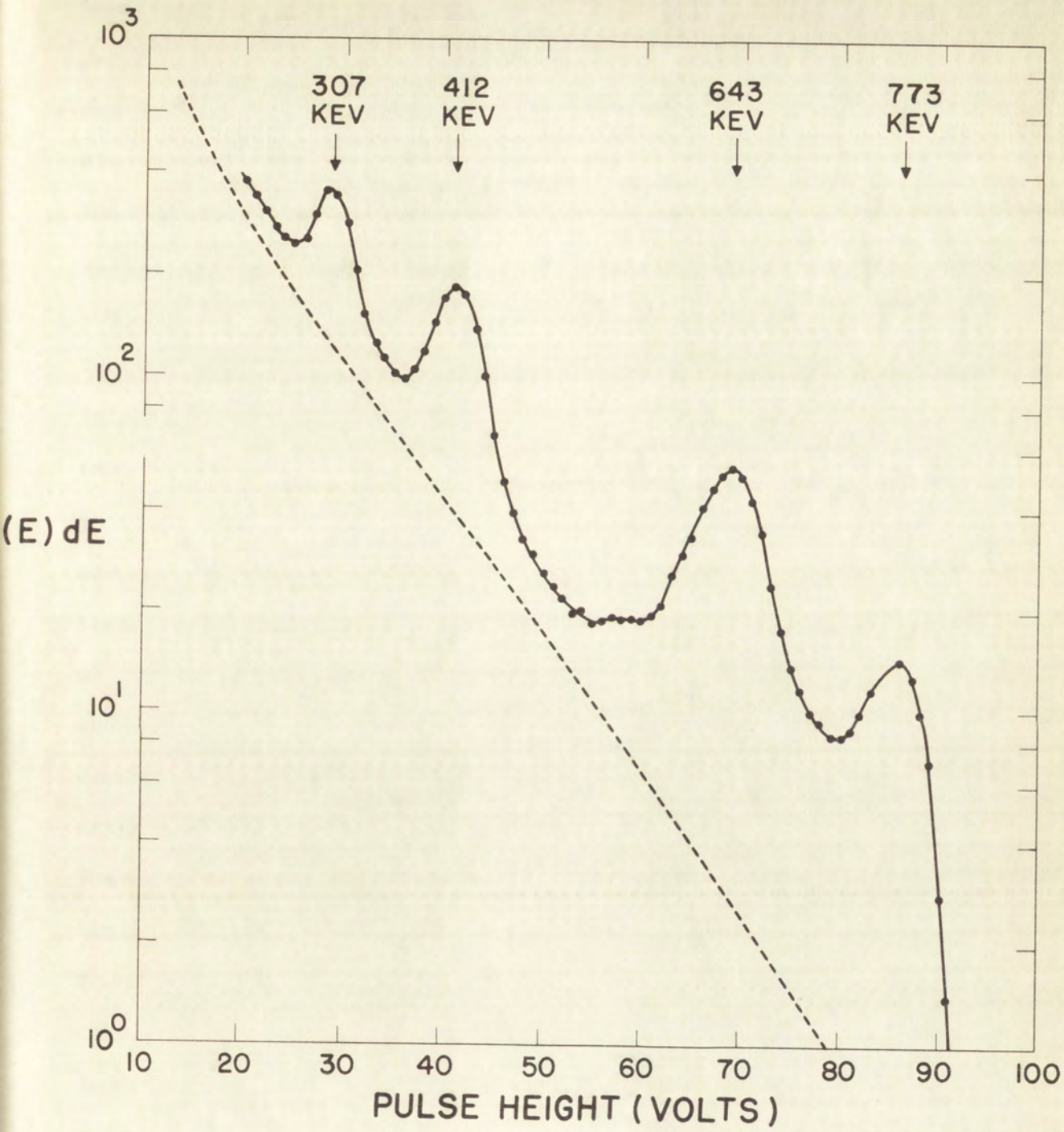

Fig. 14. Pd^{109} photon spectrum, as measured through 1/8-inch of lead. The dashed curve is the estimated bremsstrahlung contribution.

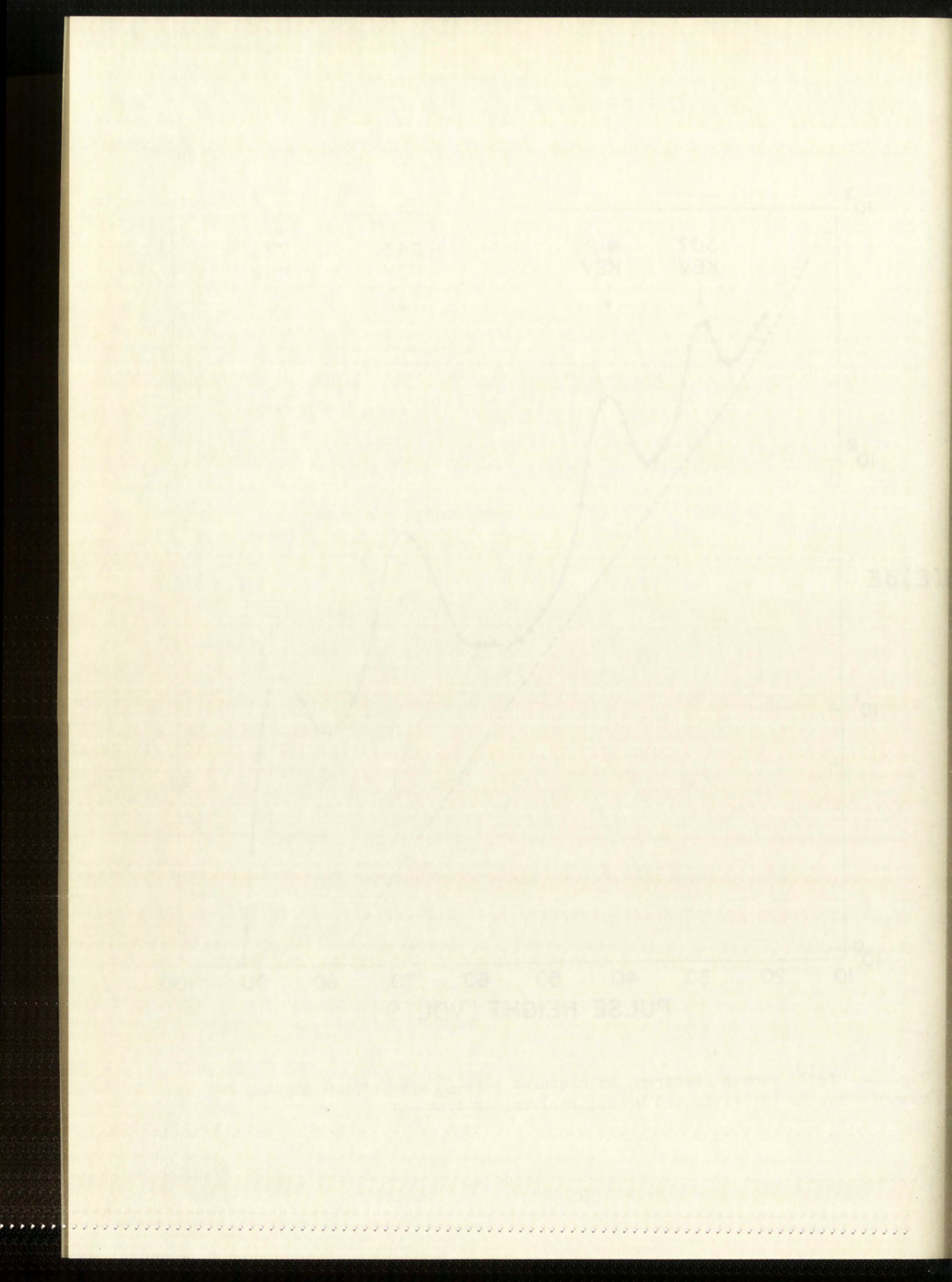

associated with the 1.0 Mev beta group of Pd^{109}. The fact that the γ-ray photopeaks are less intense than the underlying bremsstrahlung distribution is an immediate empirical indication that the observed γ rays have intensities $<<10^{-2}$ per disintegration. To obtain the energies and relative intensities of the observed γ rays, it was necessary to carefully "unfold" the spectrum, using standardized pulse-height distributions obtained with monoenergetic γ-ray sources. These distributions were subtracted from the raw data until only the monotonically decreasing bremsstrahlung distribution remained. In Fig. 15 are shown the data obtained after subtraction of the bremsstrahlung distribution. The indicated photopeaks were resolved by the described unfolding procedure. The intensity (in terms of γ rays per disintegration) of each of the observed γ rays was obtained from the measured ratio of the emission rates of these γ rays to the source decay rate. The γ-ray emission rates were determined by dividing the measured areas of the photopeaks shown in Fig. 15 by the appropriate detection efficiencies obtained from Fig. 3. The source decay rate was determined as follows: The source used for the preceding γ-ray measurements was dissolved and diluted to 20 ml. A 0.020 ml aliquot of this solution was absolute beta counted using a methane flow proportional counter. This counter had a measured detection efficiency of 56.5% for a beta-ray spectrum of 1.0-Mev end-point energy. The conversion electrons from the 88-kev isomeric transition were stopped in the counter window, and the counting rate resulting from the detection of γ rays was found to be completely negligible. The data were corrected for natural background and for counting-loss due to the finite resolving time of the counter. The source decay rate at the time when the γ-ray intensity measurements were made was then calculated from the corrected beta counting rate, taking into account the beta detection efficiency, the fraction of the source counted, and the amount of source decay between the times of gamma counting and beta counting. The results of this analysis are presented in Table IV.

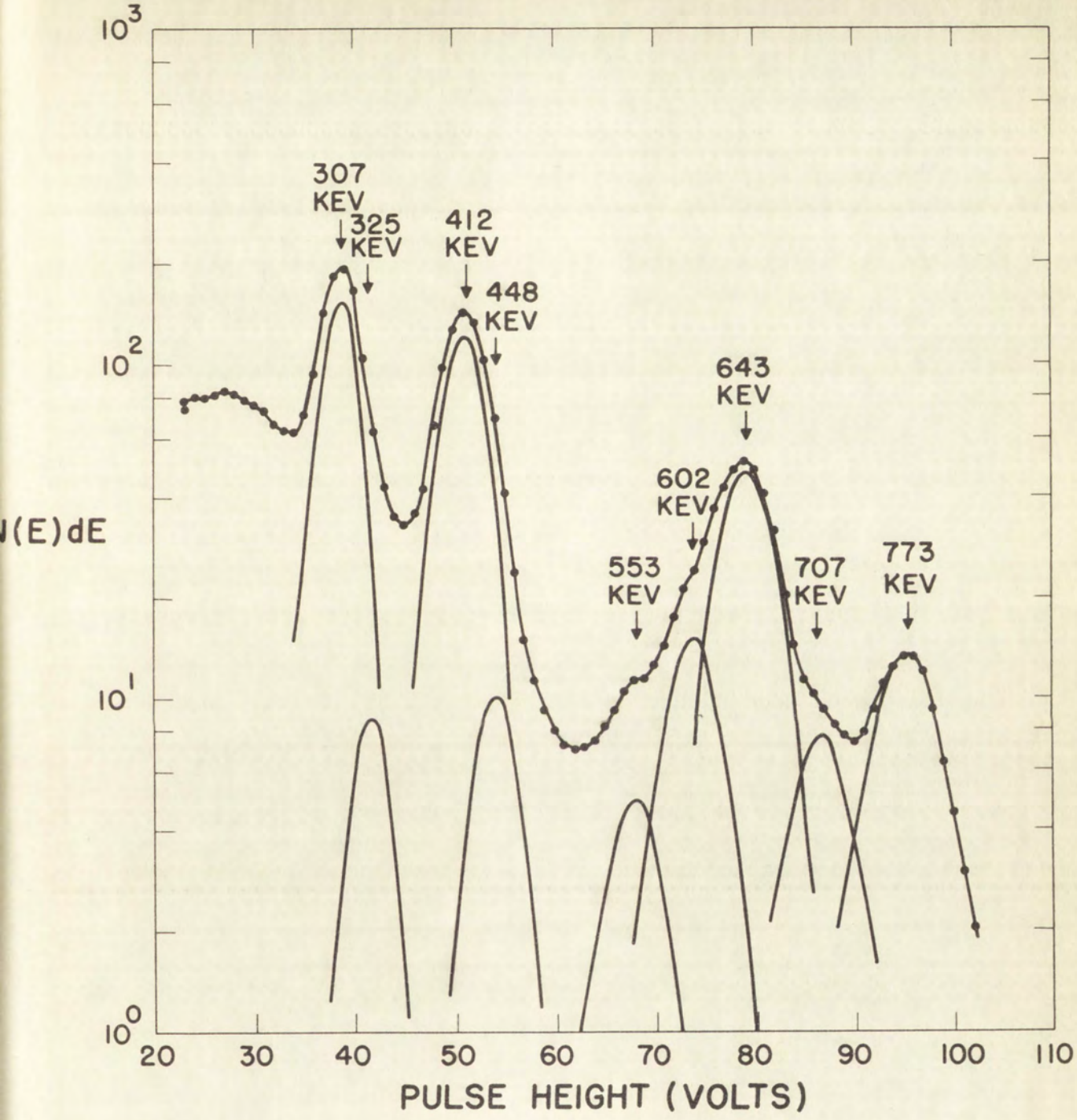

Fig. 15. Pd^{109} γ-ray spectrum, showing the "unfolded" γ-ray photopeaks.

TABLE IV. Energies and intensities of the Pd^{109} γ rays resolved in the experiment of Fig. 15.

E_γ (kev)	Intensity (γ rays per 10^5 disintegrations)
773	3.9
707	2.0
643	9.4
602	2.6
553	1.8
448	1.0
412	11.7
332	0.7
307	11.5

4.6 Gamma-Gamma Coincidence Experiments. γ-γ coincidence measurements were performed to examine genetic relationships among the various γ rays. The procedure used was as follows: A Pd^{109} source was placed between two NaI detectors which were mounted with axial symmetry axes at 180° with respect to one another. The detectors were mounted as close together as permitted by the dimensions of the source and the absorbers placed between the source and each detector. Unless otherwise noted, the absorbers were 1/4 in. of lucite, 0.020 in. of lead, 0.015 in. of cadmium, and 0.005 in. of copper. In Fig. 16, the two detectors are shown in place on the spectrometer table. In γ-γ coincidence experiments of the type described below, pulses from detector No. 1 (as identified in Fig. 6) are analyzed only when the analyzer is gated by a pulse from the coincidence circuit. Thus, the observed coincidence spectrum represents the γ-ray spectrum which is coincident with selected pulses from detector No. 2, designated as "gate" pulses. In general, the No. 2 coincidence channel is set

associated with the 1.0 Mev beta group of Pd^{109}. The fact that the γ-ray photopeaks are less intense than the underlying bremsstrahlung distribution is an immediate empirical indication that the observed γ rays have intensities $<<10^{-2}$ per disintegration. To obtain the energies and relative intensities of the observed γ rays, it was necessary to carefully "unfold" the spectrum, using standardized pulse-height distributions obtained with monoenergetic γ-ray sources. These distributions were subtracted from the raw data until only the monotonically decreasing bremsstrahlung distribution remained. In Fig. 15 are shown the data obtained after subtraction of the bremsstrahlung distribution. The indicated photopeaks were resolved by the described unfolding procedure. The intensity (in terms of γ rays per disintegration) of each of the observed γ rays was obtained from the measured ratio of the emission rates of these γ rays to the source decay rate. The γ-ray emission rates were determined by dividing the measured areas of the photopeaks shown in Fig. 15 by the appropriate detection efficiencies obtained from Fig. 3. The source decay rate was determined as follows: The source used for the preceding γ-ray measurements was dissolved and diluted to 20 ml. A 0.020 ml aliquot of this solution was absolute beta counted using a methane flow proportional counter. This counter had a measured detection efficiency of 56.5% for a beta-ray spectrum of 1.0-Mev end-point energy. The conversion electrons from the 88-kev isomeric transition were stopped in the counter window, and the counting rate resulting from the detection of γ rays was found to be completely negligible. The data were corrected for natural background and for counting-loss due to the finite resolving time of the counter. The source decay rate at the time when the γ-ray intensity measurements were made was then calculated from the corrected beta counting rate, taking into account the beta detection efficiency, the fraction of the source counted, and the amount of source decay between the times of gamma counting and beta counting. The results of this analysis are presented in Table IV.

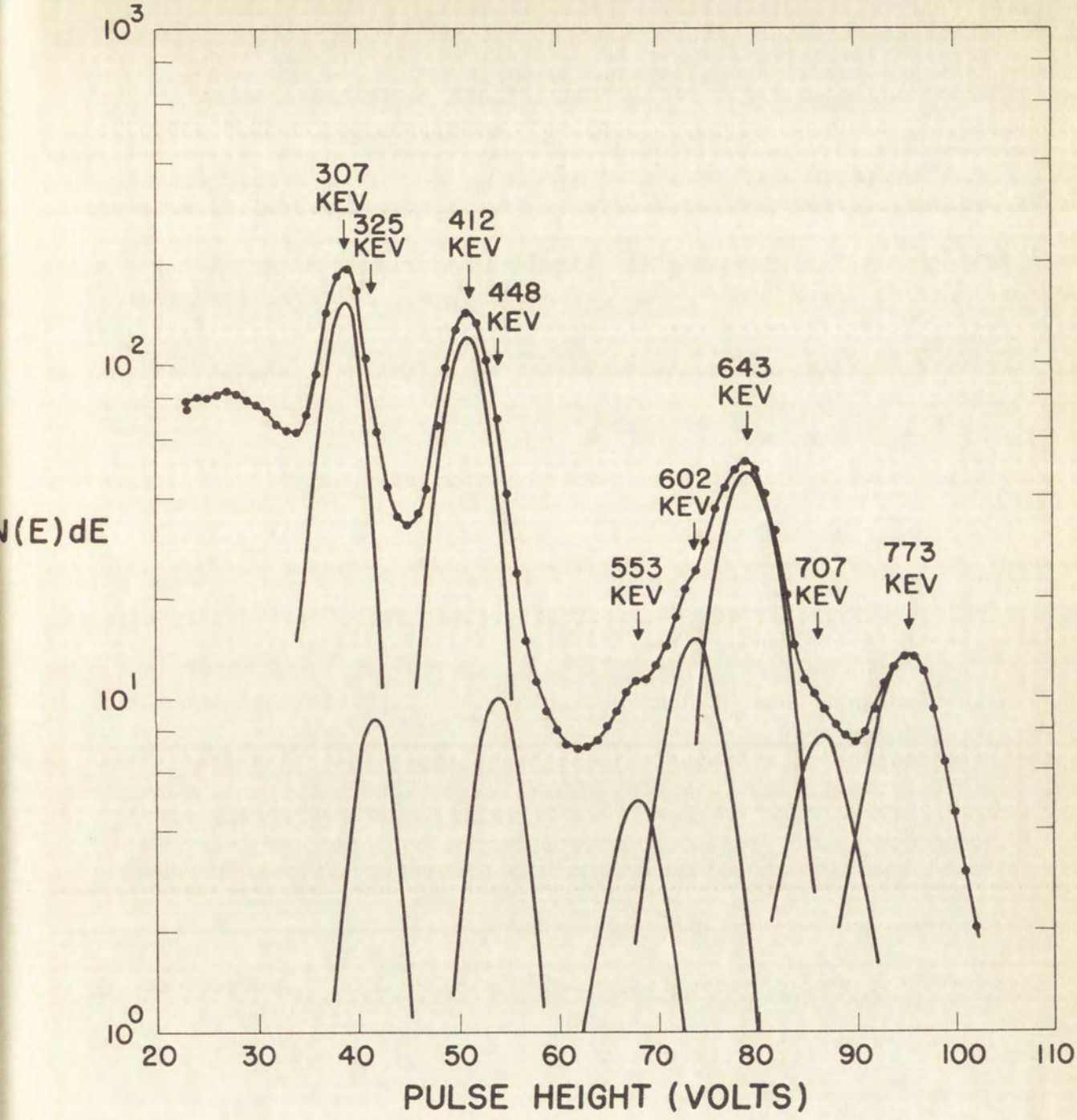

Fig. 15. Pd^{109} γ-ray spectrum, showing the "unfolded" γ-ray photopeaks.

TABLE IV. Energies and intensities of the Pd^{109} γ rays resolved in the experiment of Fig. 15.

E_γ (kev)	Intensity (γ rays per 10^5 disintegrations)
773	3.9
707	2.0
643	9.4
602	2.6
553	1.8
448	1.0
412	11.7
332	0.7
307	11.5

4.6 Gamma-Gamma Coincidence Experiments. γ-γ coincidence measurements were performed to examine genetic relationships among the various γ rays. The procedure used was as follows: A Pd^{109} source was placed between two NaI detectors which were mounted with axial symmetry axes at 180° with respect to one another. The detectors were mounted as close together as permitted by the dimensions of the source and the absorbers placed between the source and each detector. Unless otherwise noted, the absorbers were 1/4 in. of lucite, 0.020 in. of lead, 0.015 in. of cadmium, and 0.005 in. of copper. In Fig. 16, the two detectors are shown in place on the spectrometer table. In γ-γ coincidence experiments of the type described below, pulses from detector No. 1 (as identified in Fig. 6) are analyzed only when the analyzer is gated by a pulse from the coincidence circuit. Thus, the observed coincidence spectrum represents the γ-ray spectrum which is coincident with selected pulses from detector No. 2, designated as "gate" pulses. In general, the No. 2 coincidence channel is set

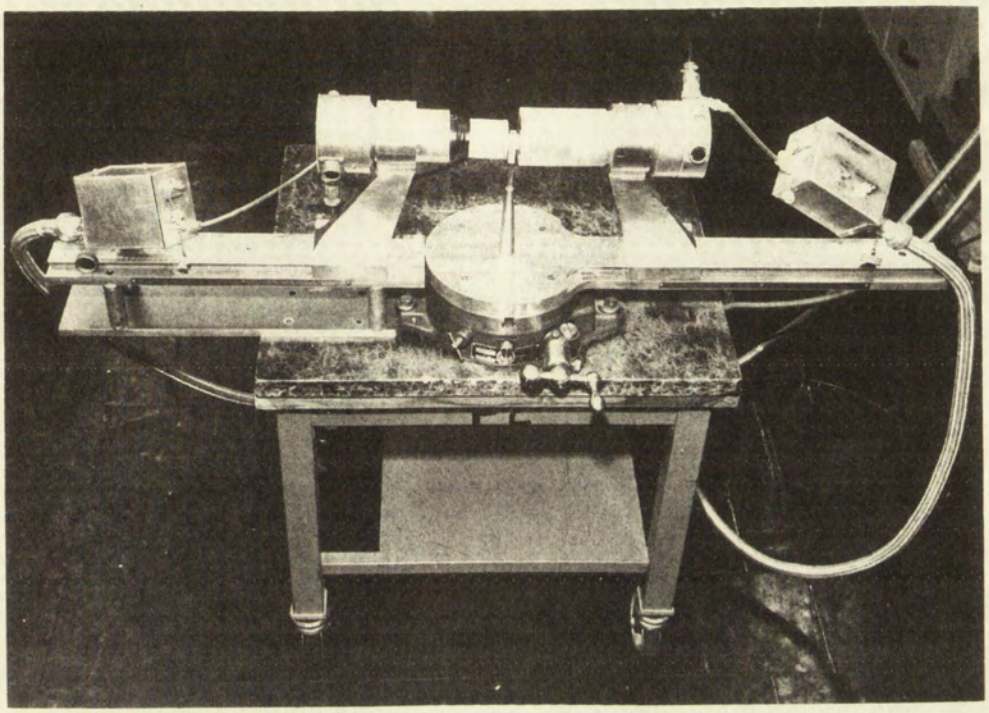

Fig. 16. Scintillation spectrometer arranged for coincidence experiments. The absorbers have been removed from the crystal on the left for better observation.

so that the majority of the "gate" pulses are associated with a single γ ray. This is accomplished by adjusting the variable lower- and upper-bound descrimination levels to span the range of pulse heights of a specific photopeak in the non-coincident (or "ungated") spectrum. This range of pulse heights is referred to as the "gate interval".

No coincidences were observed involving γ rays of energy greater than 643 kev. When the "gate interval" was centered on the 643 kev photopeak, coincidences were observed with γ rays of energy 41, 129, and 307 kev. The high energy portion of this spectrum is presented in Fig. 17. In order to determine which of the observed γ rays is actually coincident with the 643-kev γ ray, additional coincidence measurements were performed in which the "gate interval" was centered, in turn, on each of the three indicated photopeaks. When the "gate interval" was centered on either the 41- or 307-kev photopeaks, no coincidence peak was observed at 643 kev; however, when the "gate" was centered on the 129-kev photopeak, a composite peak was observed which was resolved into components of energy 602 and 643 kev. Thus, it appears that the 129-kev γ-ray is the only γ-ray in coincidence with the 643-kev γ-ray. From the experimentally measured quantities it is possible to show that the 129-kev transition precedes the 643-kev transition. The analysis is as follows: Define R to be the ratio of the 129-kev transition rate to the 643-kev transition rate. This quantity can be expressed in terms of $N_{\gamma\gamma}$, the coincidence counting rate, N_{643}, the counting rate of 643-kev γ rays in the "gate" channel, E_{129}, the detection efficiency for 129-kev γ rays, and $\alpha_T(129)$, the total internal conversion coefficient for the 129-kev transition. The expression is:

$$R = \frac{N_{\gamma\gamma}}{N_{643}} \times \frac{1 + \alpha_T(129)}{E_{129}} \qquad (4.5)$$

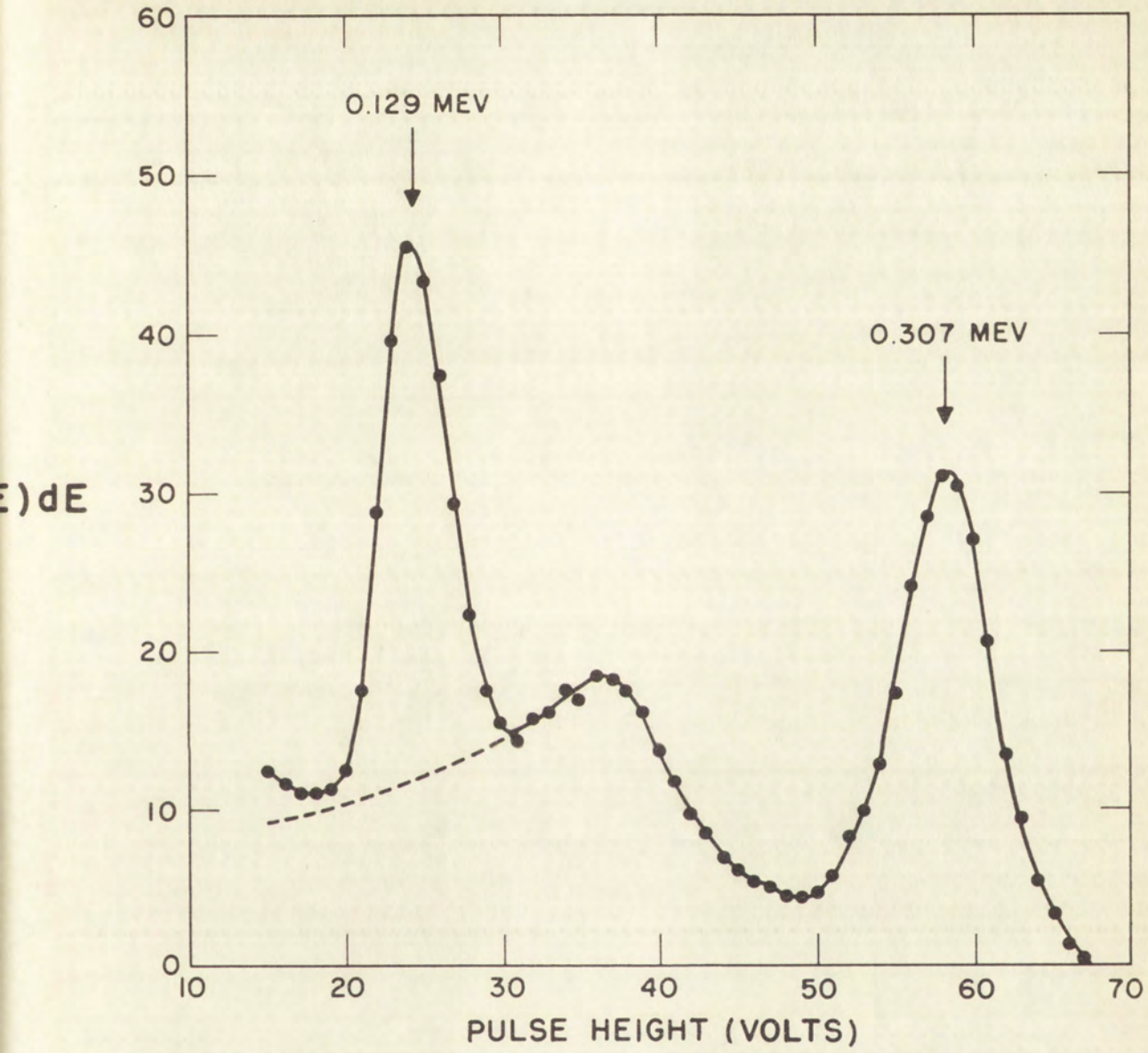

Fig. 17. High energy portion of the γ-ray spectrum of Ag^{109} in coincidence with pulses in the "gate interval" 580-710 kev.

$N_{\gamma\gamma}$ and N_{643} are experimentally measurable quantities, E_{129} is obtainable from Fig. 3, and $\alpha_T(129)$ can be estimated theoretically. Because the 129-kev transition competes measurably with the 773-, 553-, and 448-kev transitions (Sec. 5.1), it must be a very fast, low-multipole transition: i.e., M1, E1 or E2. For these three multipolarity assignments, $\underline{R}$ is calculated to be 0.05, 0.04, and 0.06, respectively. Inasmuch as the only transition in coincidence with the 643-kev γ ray is that of 129 kev, and as $\underline{R}$ is much less than unity, it follows immediately that the 129-kev γ ray precedes the 643-kev γ ray.

In the preceding series of experiments, when the "gate interval" was centered about the position of the 41-kev γ-ray photopeak, γ rays of energy 602, 307, 412, and 553 kev were observed. Therefore, experiments were performed in which the "gate interval" was centered, in turn, on the photopeaks of each of these γ rays. The results were as follows: (1) It was found that the 41-kev γ ray is in coincidence only with the 602-kev γ ray. (2) A 553-kev γ ray was observed in the coincidence spectrum when the "gate interval" was set to include the 307-kev photopeak, and conversely, a 307-kev photopeak was observed when the "gate interval" was set to span the 553-kev γ-ray photopeak. Thus, it is firmly established that there exists a (553-307)-kev cascade. It is now clear that the 307-kev γ ray observed when the "gate" was centered on the 643-kev photopeak resulted from the fact that part of the high-energy "tail" of the 553-kev photopeak extended into the selected "gate" region. (3) In the experiment in which the "gate interval" was centered on the 307-kev photopeak, a strong coincidence peak was observed at 412 kev (see Fig. 18). (4) The coincidence spectrum obtained when the "gate" was centered on the 412-kev photopeak revealed γ-ray photopeaks of 307, 412, and 448 kev, as shown in Fig. 19.

From the above results, it is evident that there is a (307-412)-kev γ-γ cascade involved in the decay scheme. An experiment was performed to determine the fraction of the 307 kev γ rays in coincidence with 412 kev γ rays.

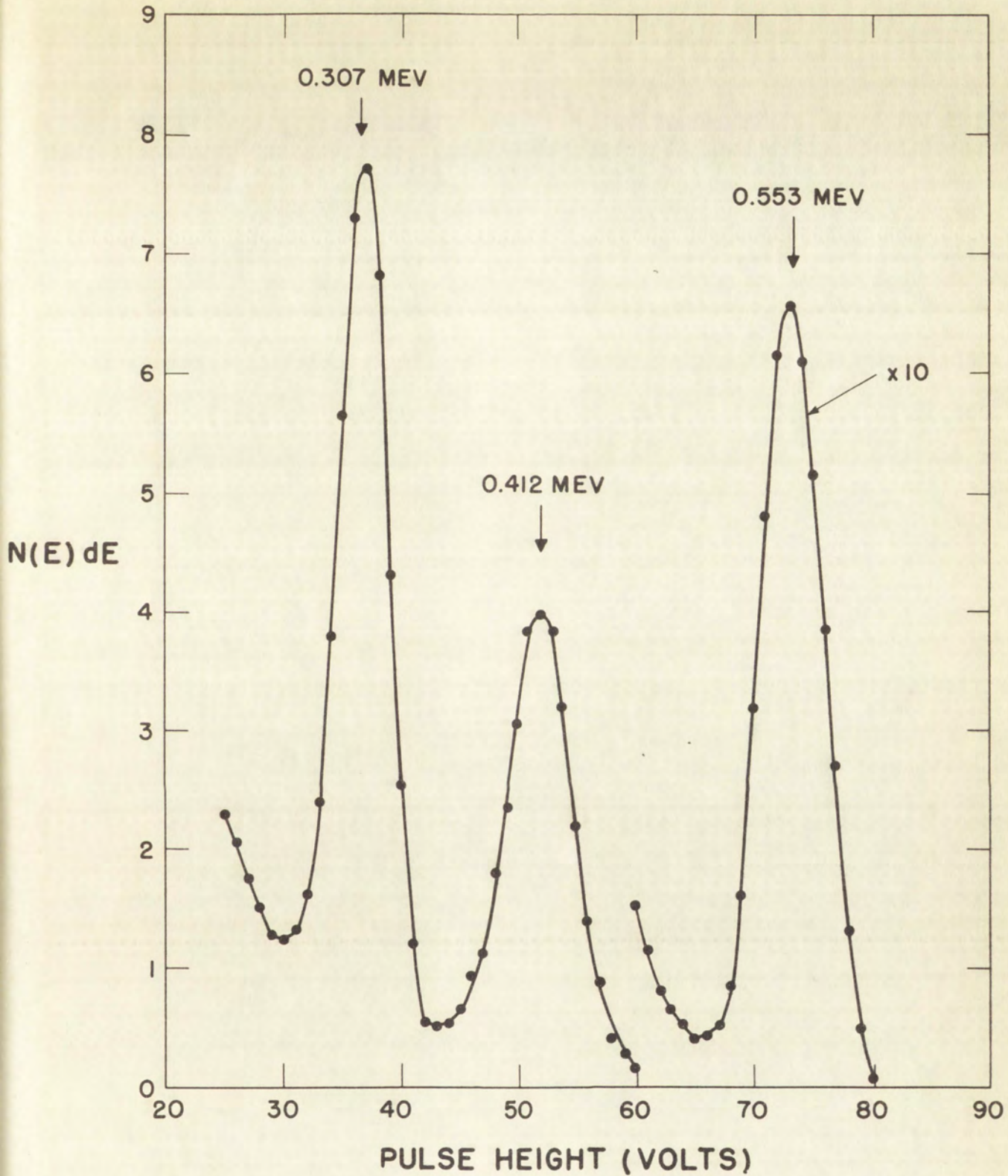

Fig. 18. Gamma-ray spectrum of Ag^{109} in coincidence with pulses in the "gate interval" 280-350 kev.

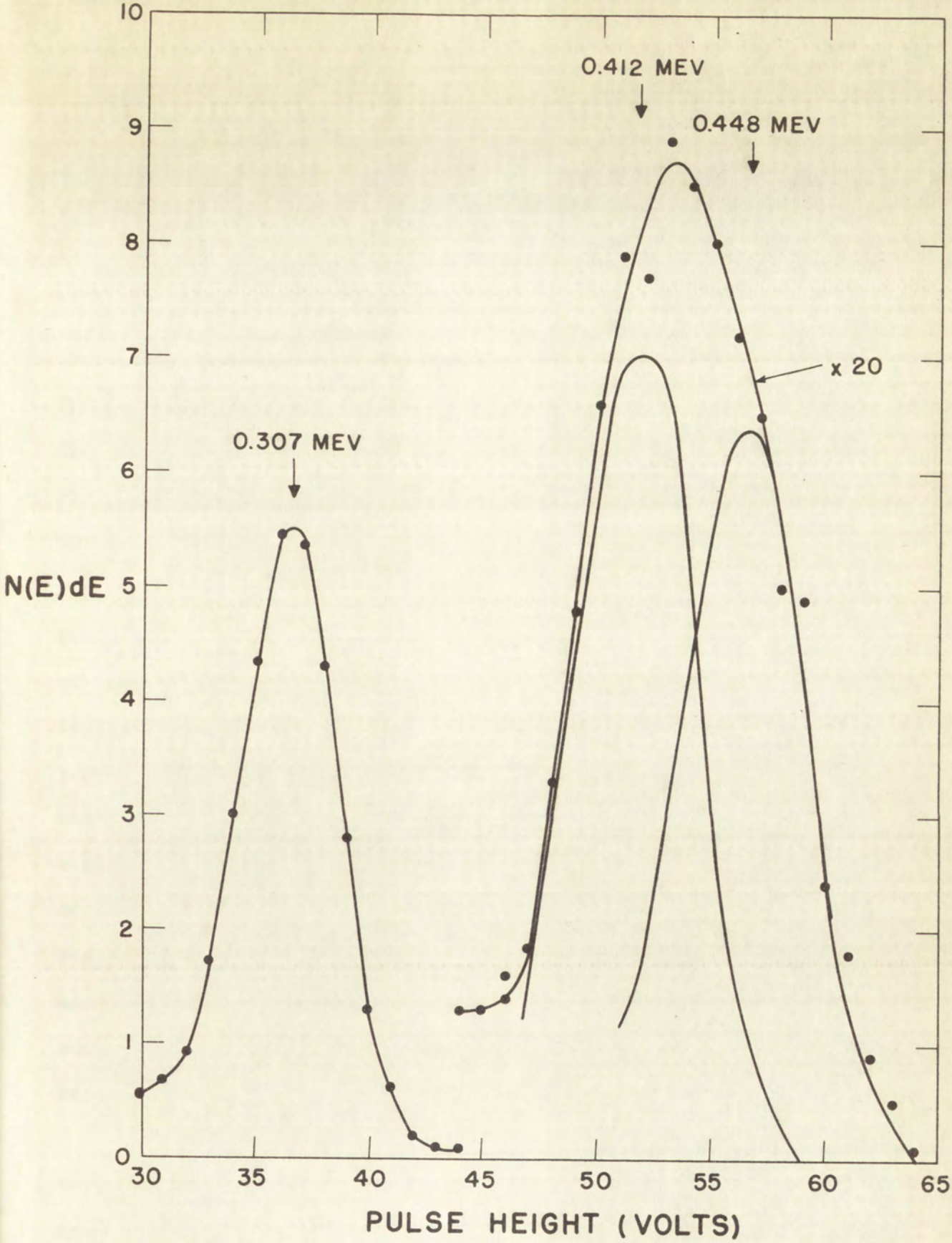

Fig. 19. Gamma-ray spectrum of Ag^{109} in coincidence with pulses in the "gate interval" 370-470 kev.

$N_{\gamma\gamma}$ and N_{643} are experimentally measurable quantities, E_{129} is obtainable from Fig. 3, and $\alpha_T(129)$ can be estimated theoretically. Because the 129-kev transition competes measurably with the 773-, 553-, and 448-kev transitions (Sec. 5.1), it must be a very fast, low-multipole transition: i.e., M1, E1 or E2. For these three multipolarity assignments, $\underline{R}$ is calculated to be 0.05, 0.04, and 0.06, respectively. Inasmuch as the only transition in coincidence with the 643-kev γ ray is that of 129 kev, and as $\underline{R}$ is much less than unity, it follows immediately that the 129-kev γ ray precedes the 643-kev γ ray.

In the preceding series of experiments, when the "gate interval" was centered about the position of the 41-kev γ-ray photopeak, γ rays of energy 602, 307, 412, and 553 kev were observed. Therefore, experiments were performed in which the "gate interval" was centered, in turn, on the photopeaks of each of these γ rays. The results were as follows: (1) It was found that the 41-kev γ ray is in coincidence only with the 602-kev γ ray. (2) A 553-kev γ ray was observed in the coincidence spectrum when the "gate interval" was set to include the 307-kev photopeak, and conversely, a 307-kev photopeak was observed when the "gate interval" was set to span the 553-kev γ-ray photopeak. Thus, it is firmly established that there exists a (553-307)-kev cascade. It is now clear that the 307-kev γ ray observed when the "gate" was centered on the 643-kev photopeak resulted from the fact that part of the high-energy "tail" of the 553-kev photopeak extended into the selected "gate" region. (3) In the experiment in which the "gate interval" was centered on the 307-kev photopeak, a strong coincidence peak was observed at 412 kev (see Fig. 18). (4) The coincidence spectrum obtained when the "gate" was centered on the 412-kev photopeak revealed γ-ray photopeaks of 307, 412, and 448 kev, as shown in Fig. 19.

From the above results, it is evident that there is a (307-412)-kev γ-γ cascade involved in the decay scheme. An experiment was performed to determine the fraction of the 307 kev γ rays in coincidence with 412 kev γ rays.

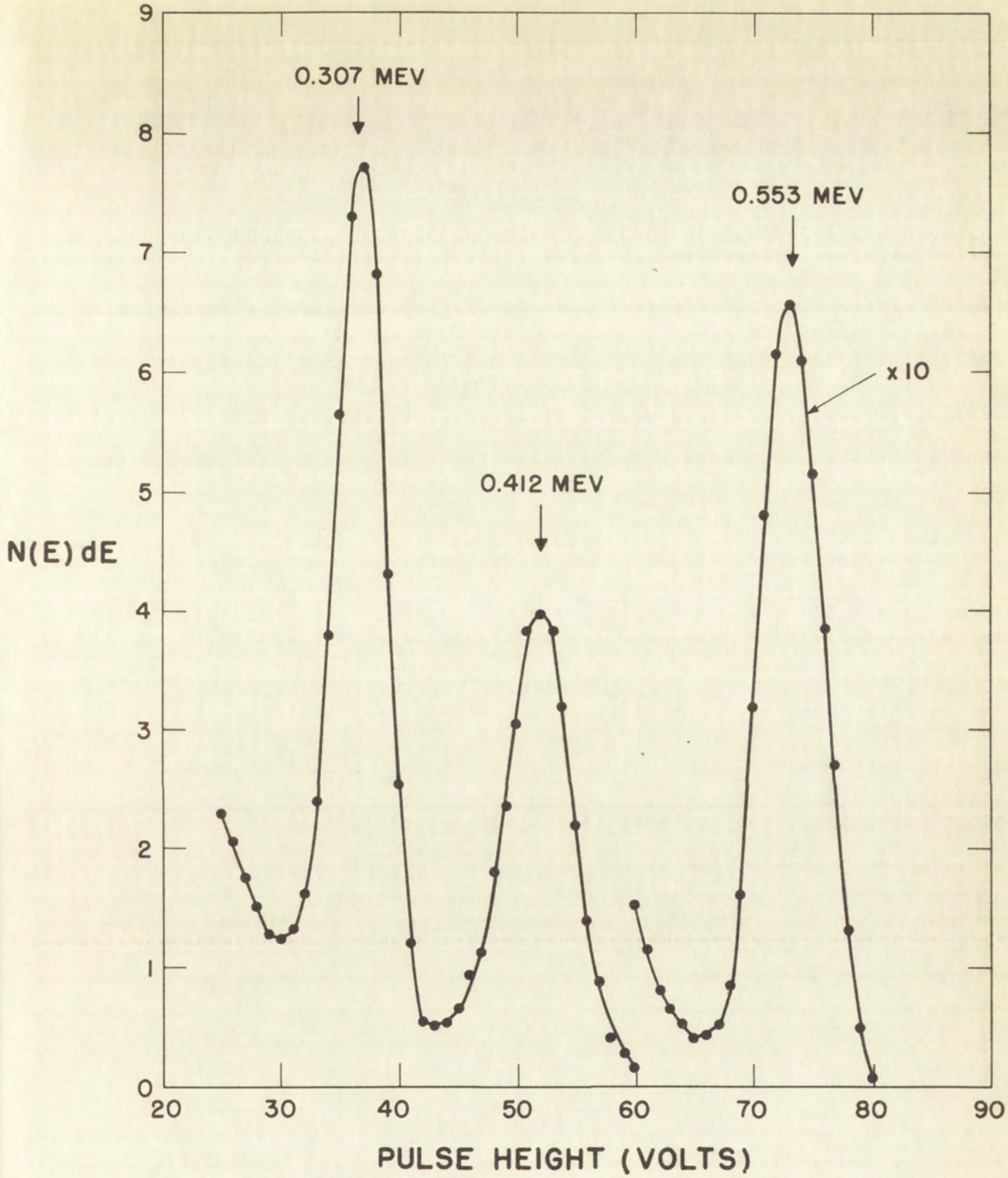

Fig. 18. Gamma-ray spectrum of Ag^{109} in coincidence with pulses in the "gate interval" 280-350 kev.

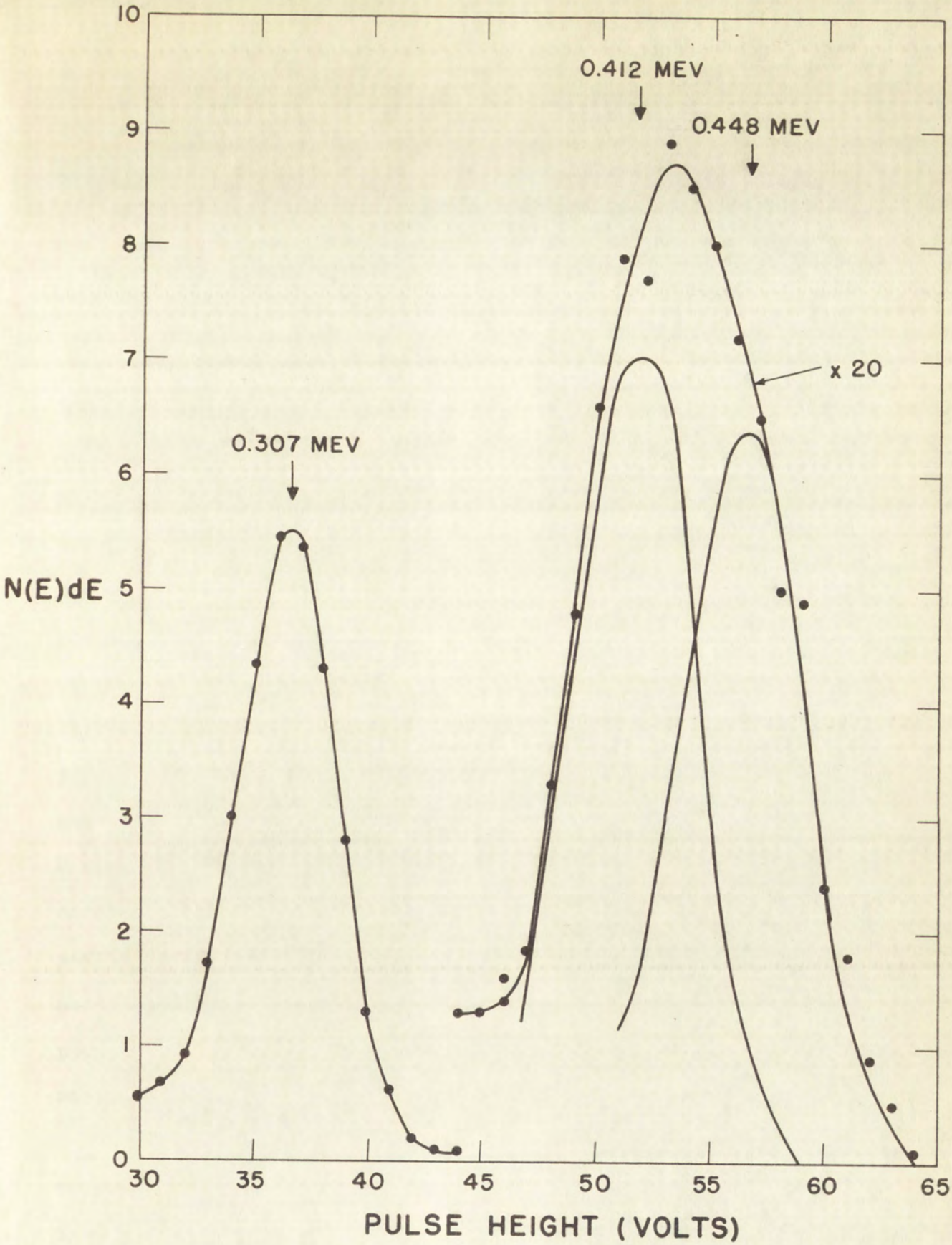

Fig. 19. Gamma-ray spectrum of Ag^{109} in coincidence with pulses in the "gate interval" 370-470 kev.

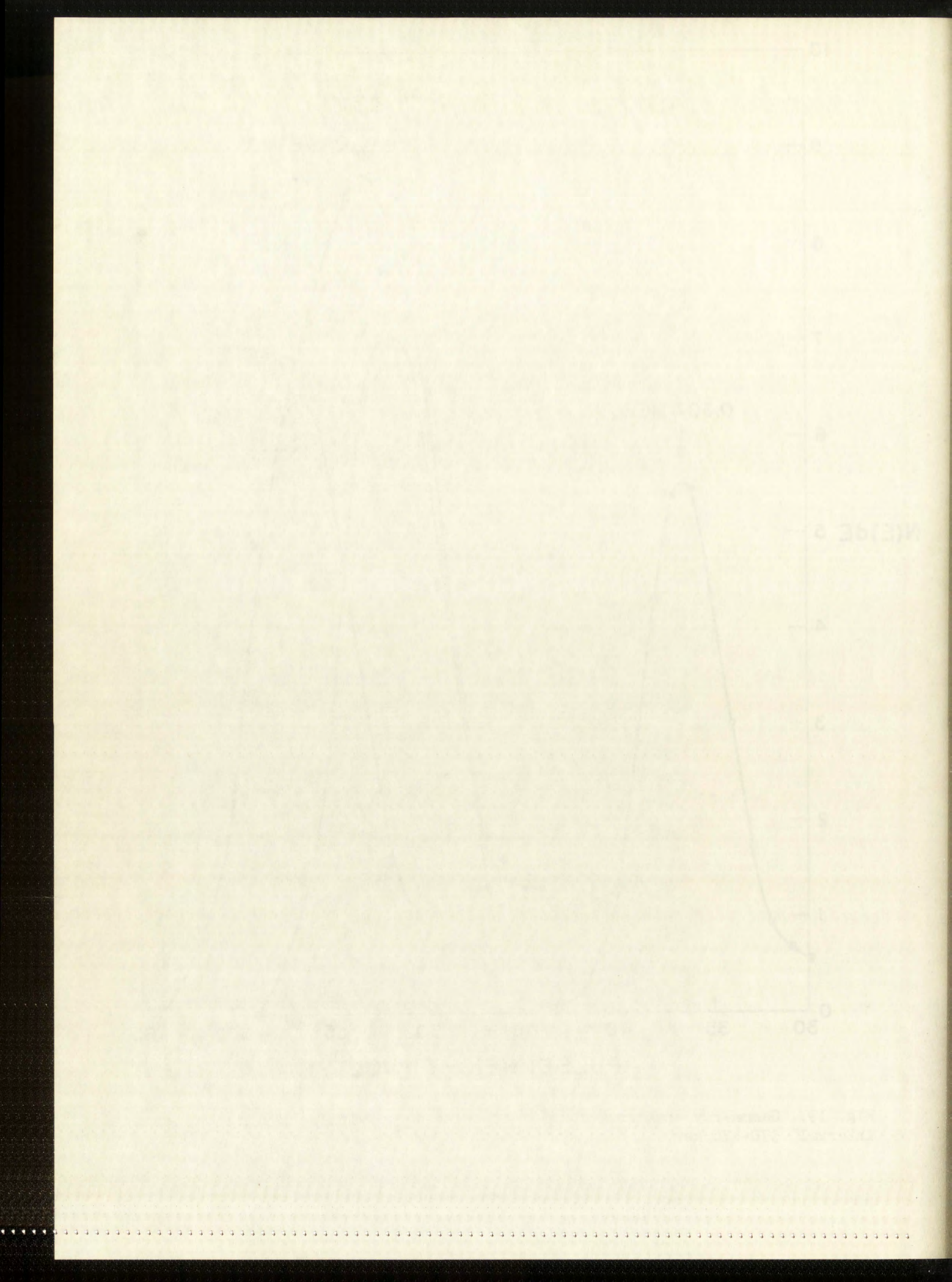

This fraction, f, is expressible in terms of N_c (the counting rate of coincidences between 307- and 412-kev γ rays), N_{412} (the counting rate of 412-kev γ rays in the "gate interval"), and E_{307} (the detection efficiency of the "analyser" crystal for 307-kev γ rays) as follows:

$$f = \frac{N_c}{N_{412} E_{307}} . \qquad (4.6)$$

The correction for internal conversion of the 307-kev γ ray is negligible. The counting rates were experimentally measured and E_{307} was obtained from Fig. 3. The value of f obtained is 0.65 ± 0.15. Of the remaining 35% of the 307 kev γ rays, 12% are accounted for by the (307-553)-kev γ-γ coincidence. The 23% of the 307-kev γ rays which are not involved in any γ-ray cascade must result from direct beta decay to the 307-kev level. Since one of the γ rays of the (307-412)-kev γ-ray cascade is presumably a ground state transition, it follows that there must be a level at 719 kev which decays by emission of γ rays of 307- and/or 412-kev, which in turn populate the level(s) at 412- and/or 307-kev. Thus, it is certain that one (and quite possibly both) of the observed 307- and 412-kev photopeaks of Fig. 18 is induced by a pair of γ rays of very nearly the same energy. In none of the experiments performed was it possible to separately resolve these nearly-degenerate γ rays; consequently, accurate energies and intensities of the two possible ~307-kev γ rays and two possible ~412-kev γ rays are not known. All of the observed γ-γ coincidence relationships are listed in Table V.

Since the 88-kev level has a 41-sec half-life, it was not possible to use coincidence techniques to determine which γ-ray transitions populate this level.

In this study it has been impossible to determine the multipolarity of any of the newly-observed transitions. Transition multipolarities are usually

TABLE V. Summary of the observed γ-γ coincidence relationships.

(1) γ-ray energy (kev)	(2) γ-rays verified to be coincident with γ rays in column (1) (kev)
41	602
129	602, 643
307	412, 553
412	307, 448
448	412
553	307
602	41, 129
643	129

determined from conversion-electron data (α_K, K/L ratios, and L-subshell conversion ratios) or photon intensity data (α_K). In the present study, all of the observed transitions (except the 88-kev transition) have such extremely low intensities per disintegration that their conversion lines cannot be observed in the presence of the Pd^{109} beta-ray continuum. Determination of α_K for any specific transition by photon studies requires measurement of the ratio of the number of γ rays emitted to the number of K x-rays emitted following K internal-conversion of the transition. Because of the numerous γ-rays in the Pd^{109} spectrum, the only way to measure the number of K x-rays engendered by a specific transition is by the coincidence method. It is essential to this method that it be possible to select a "gate interval" such that all of the coincidences analyzed result from the transition under investigation. This condition is not met in these studies.

CHAPTER V

INTERPRETATION OF EXPERIMENTAL RESULTS

5.1 The Decay Scheme. A decay scheme consistent with the data presented above is shown in Fig. 20. The principal arguments which support this scheme are discussed below.

Pd^{109m} was observed to decay only by a 188-kev transition to the ground state. The upper limit on the fraction of the Pd^{109m} disintegrations which proceed by beta decay was estimated to be 0.2%.

The principal decay branch of the Pd^{109} ground state is the beta-ray group of end-point energy 1.025 Mev, which has been shown to populate the 88-kev level in Ag^{109}. The other indicated beta-ray groups were not observed; their energies and intensities were deduced from the γ-ray data.

The previously-mentioned coulomb-excitation studies have established the existence of levels in Ag^{109} at 307 and 412 kev. As discussed in Sec. 4.6, the strong (307-412)-kev γ-γ coincidence observed in the present experiments is interpreted to mean that there is a level at 719 kev which decays to one or both of the known levels at 307 and 412 kev. The experimental data yield no information on the relative strength of the two possible (307-412)-kev cascades.

The observed (307-553)- and (412-448)-kev γ-γ coincidences both indicate the existence of a level at 860 kev. The 773-kev γ ray is assigned to be the transition from the 860-kev level to the 88-kev level. There are two reasons for this assignment: (1) The difference in energy of the 860- and 88-kev levels is 732 kev which is, within experimental error, the energy of the γ ray observed. (2) The 773-kev γ ray was not observed to be in coincidence with other γ rays. It must therefore either populate the 88-kev level, as postulated, or be a ground-state transition. If it were a ground-state transition, there should also be a transition of comparable intensity to the 307-kev level. This

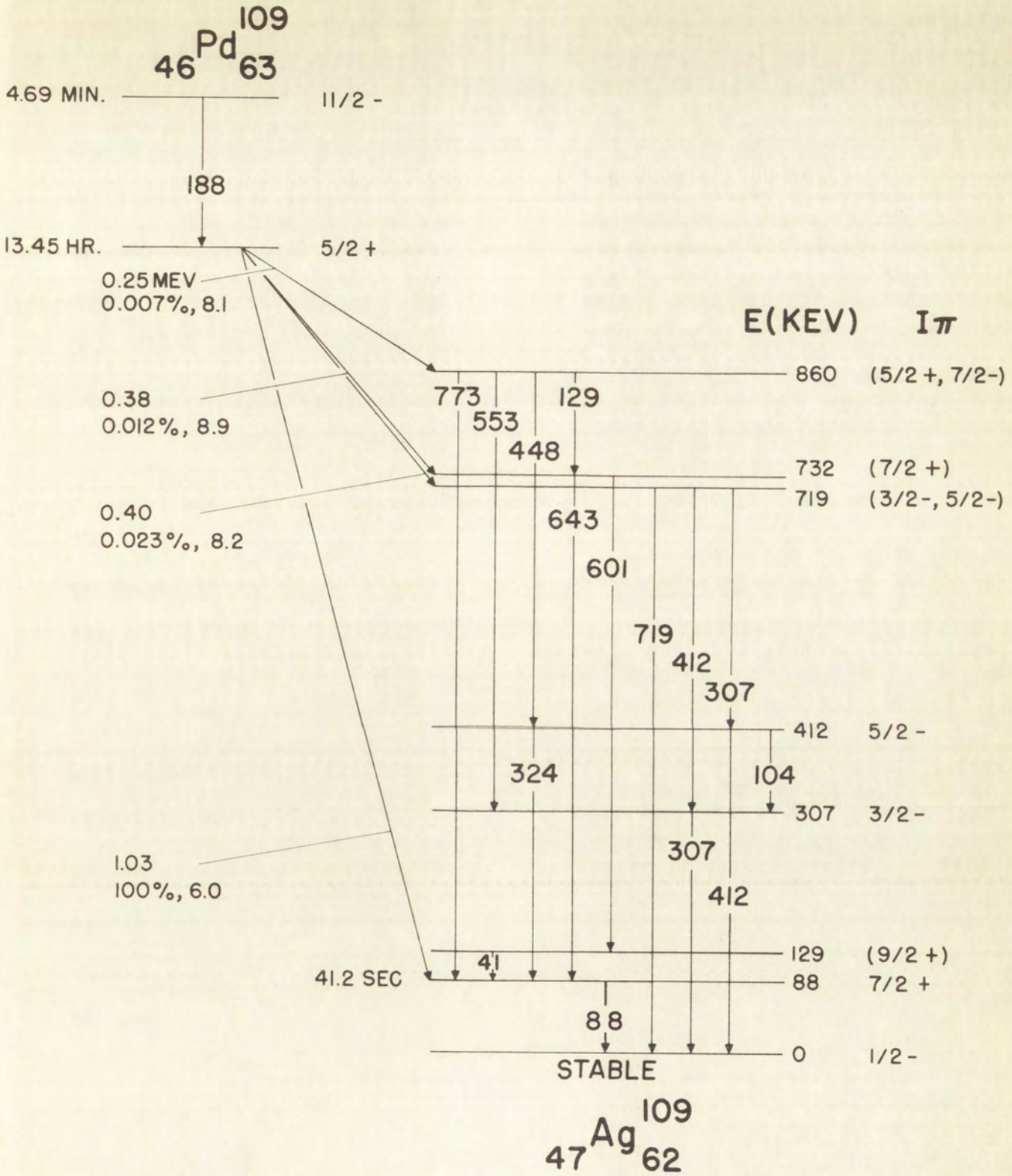

Fig. 20. Proposed decay scheme of Pd^{109m} and Pd^{109}.

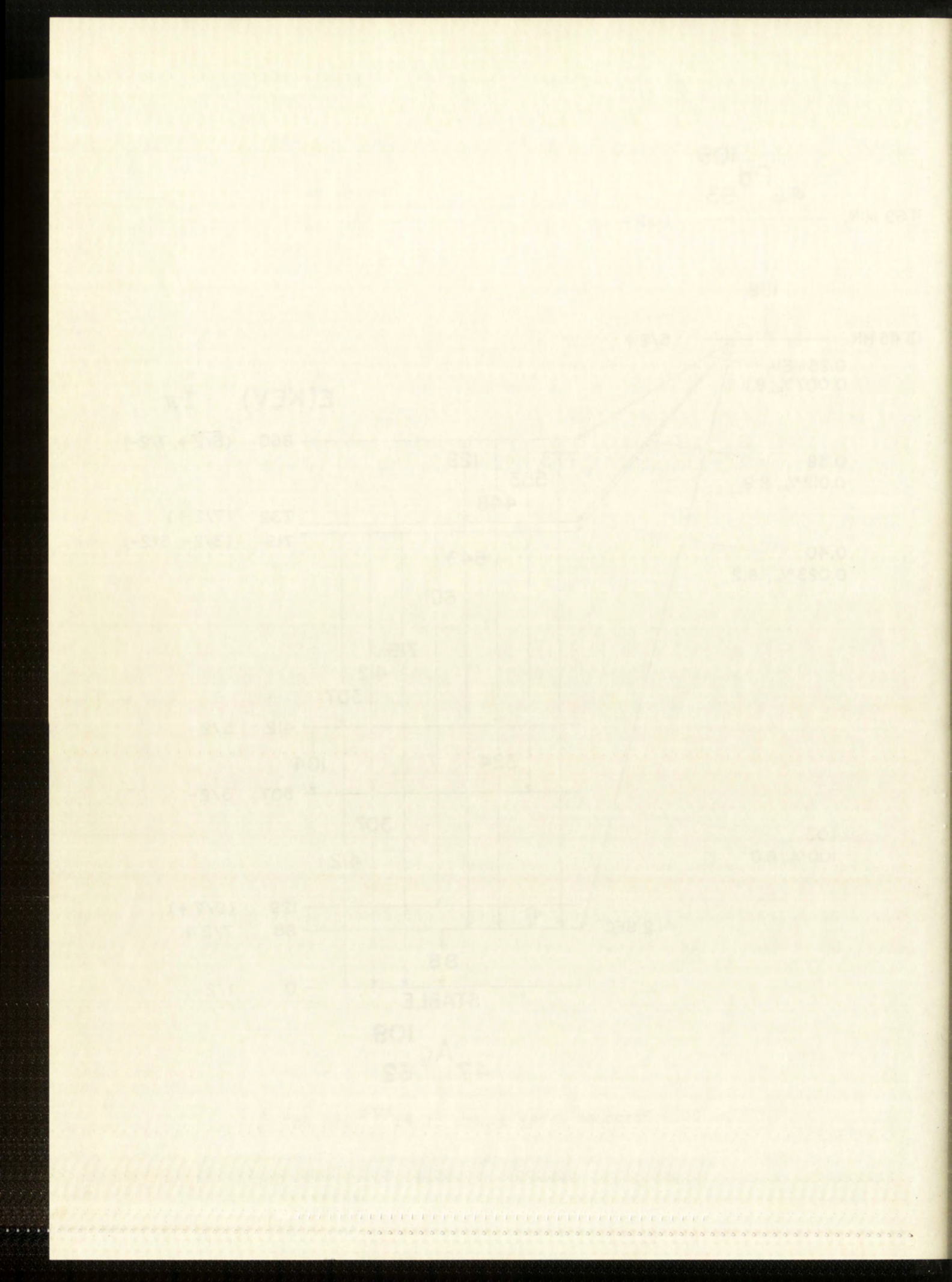

transition would be detected as a (307-466)-kev γ-γ coincidence. No such coincidence was observed.

The (129-643)-kev γ-ray cascade is believed to parallel the 773-kev γ ray. The fact that the 129-kev γ ray precedes the 643-kev γ ray (see Sec. 4.6) leads to the postulation of a level at 732 kev.

The established (602-41)- and 602-129)-kev γ-γ coincidence relationships indicate that the (602-41)-kev γ-ray cascade parallels the 643-kev transition. It has not been possible to determine experimentally the order of the 602- and 41-kev γ rays in this cascade. For reasons which are discussed in Section 5.3, the 602-kev transition is thought to precede the 41-kev transition.

The only γ ray not yet assigned is that of 707 kev. Because this γ ray is not observed in any coincidence measurement, it must populate either the 88-kev level or the ground state. In view of the large uncertainty in the energy of this gamma ray, it seems possible that it could be the cross-over transition from the 719-kev level to the ground state.

5.2 State Assignments in Pd^{109}. The ground state of Pd^{109} has been shown to beta decay to the 7/2+ state in Ag^{109}. The value of log ft for this transition is calculated to be 6.0, which indicates that the transition is probably of the "allowed" type; i.e., $\Delta I = (0, \pm 1)$, $\Delta\pi$ = no. The spin and parity of Pd^{109} are thereby limited to the choices 5/2+, 7/2+, or 9/2+. The Pd^{109m} isomeric transition has been shown to be of multipolarity E3. This fact indicates that the two Pd^{109} isomers differ in spin by 3 units and have opposite parities.

Shell model states which meet the above requirements are available for assignment to the two levels in question. The ground state neutron configuration for Pd^{109} predicted by the shell model is $(\quad)^{50}(1g_{7/2})^{8}(2d_{5/2})^{5}$, $I = 5/2$. Among the anticipated low-lying states are those arising from excitation of the odd $d_{5/2}$ neutron to the $d_{3/2}$, $s_{1/2}$, or $h_{11/2}$ shells, states having

I = 3/2+, 1/2+, and 11/2-, respectively. Since the only negative parity state available is the 11/2- state, Pd^{109m} is assigned to have I = 11/2-. The E3 character of the isomeric transition then forces Pd^{109} to have I = 5/2+, in agreement with the shell-model prediction.

5.3 State Assignments in Ag^{109}. The spin and parity of the low-lying states in $_{47}Ag_{62}^{109}$ will, as mentioned in Section 2.2, be determined primarily by the proton core. The shell model, interpreted literally, would predict the proton configuration for the ground state of Ag^{109} to be $(\quad)^{38}(2p_{1/2})^2(1g_{9/2})^7$, I = 9/2+. The small spacing between the $2p_{1/2}$ and $1g_{9/2}$ shells and the strong j dependence of pairing energy make the configuration $(\quad)^{38}(1g_{9/2})^8(2p_{1/2})^1$, I = 1/2-, an equally likely configuration for the ground state. The ground-state spin has been measured to be 1/2. The latter configuration is therefore that of the ground state, while the former configuration is expected to be that of a very low-lying level.

As mentioned before, Coulomb excitation experiments have established the existence of a 1/2-, 3/2-, 5/2- rotational band based on the ground state. Occurrence of rotational structure implies rather large nuclear deformation and strong mixing of shell-model type wave functions. Therefore, although the ground state may be predominantly the configuration discussed above, it is expected to contain sizeable admixtures of other states of spin 1/2 associated with the odd proton orbitals $f_{5/2}$, $p_{3/2}$, and $f_{7/2}$.

From the experiments which established the existence of the ground-state rotational band, the reduced transition probabilities B(E2) for the 307- and 412-kev transitions were obtained. The reported values are B(E2; 307) = 0.17×10^{-48} e^2cm^2 and B(E2; 412) = 0.31×10^{-48} e^2cm^2. The static nuclear

deformation β can be determined from the reduced transition probability by means of the relations[45]

$$Q_o^2 = \frac{9}{5\pi} Z^2 R_o^4 \beta^2 (1 + 0.16 \beta)^2 \qquad (5.1)$$

$$B(E2) = \frac{5}{16\pi} e^2 Q_o^2 \langle I_i 2K0 \mid I_i 2I_f K \rangle^2 \qquad (5.2)$$

where Z and R_o are the nuclear charge and radius respectively, and Q_o is the intrinsic quadrupole moment. The calculated values of β for the 307- and 412-kev levels are 0.17 and 0.18, respectively. It is known empirically that the transition from spherical-vibrational to rotational-collective spectra occurs at $\beta \sim 0.18$. States less strongly coupled to the surface motion than those of the K = 1/2 band would therefore not be expected to exhibit a rotational spectrum. Since the coupling-strength parameter varies as $1/\sqrt{j}$[45] and therefore has its maximum value for the ($j = 1/2$) ground state, it is anticipated that none of the other low-lying intrinsic states of Ag^{109} will have associated rotational bands.

The E3 multipolarity of the 88-kev transition establishes the spin and parity of the 88-kev level as 7/2+. Such a state is not predicted in this region by the strict single-particle shell model; however it is well known that a number of other odd-A nuclei in this region have low-lying 7/2+ states. These states are attributed to the configuration $(\quad)^{38}(2p_{1/2})^{0,2}(1g_{9/2})^{\pm 3}$. j-j coupling calculations indicate that this configuration will give rise to a multiplicity of states, the two lowest of which will have spin and parity 9/2+ and 7/2+, respectively. Empirically, the 7/2+ state is lower than the 9/2+ state in approximately half the cases. Thus, the primary configurational component of the 88-kev state is assumed to be $(\quad)^{38}(2p_{1/2})^{2}(1g_{9/2})^{7}_{I=7/2}$.

The $(\quad)^{38}(2p_{1/2})^2(1g_{9/2})^7_{I=9/2}$ state is expected to lie very near the $(\quad)^{38}(2p_{1/2})^2(1g_{9/2})^7_{I=7/2}$ state. In the case of Rh^{103}, a nuclide whose level structure is very similar to that of Ag^{109}, the 9/2+ and 7/2+ levels are spaced 55 kev apart. It is primarily for this reason that the observed 41-kev transition is postulated to follow, rather than precede, the 602-kev transition; i.e., the proposed 129-kev level is assumed to be identifiable with the I = 9/2 state mentioned above. The observed decay properties of the 129-kev level are clearly consistent with a 9/2+ assignment. Also, the fact that the 732-kev level decays to both the 88- and 129-kev levels lends support to the assumption that these latter two levels have similar configurations.

The 719-kev level decays detectably to only the 1/2- level and to the 3/2- and/or the 5/2- levels. From the fact that they successfully compete with one another, the observed transitions must have multipolarities of M1, E1, or E2; therefore, the spin and parity of the 719-kev level is restricted to the values 1/2±, 3/2-, or 5/2-. The log ft value of 8.2 for the beta transition to the 719-kev level implies that the transition is either allowed or first forbidden, with $\Delta I = 0, \pm 1$. This restriction eliminates the 1/2± spin states from consideration. No obvious choice can be made between the 3/2- and 5/2- possibilities. Therefore, from the shell-model point of view, the 719-kev level is presumably to be identified with either the $p_{3/2}$ or $f_{5/2}$ state, both of which would be referred to as "hole" states.

The 732-kev level is observed to decay to the 7/2+ and 9/2+ levels only. Based on the plausible assumption that these two transitions are E1, E2, or M1, the possible values of spin and parity of the 732-kev level are 5/2+, 7/2±, 9/2± and 11/2+. The beta transition from Pd^{109} (5/2+) to the 732-kev level in Ag^{109} is seen to proceed with log ft = 8.9, which probably means that the transition is either allowed or first forbidden, with $\Delta I = 0, \pm 1$. This restriction eliminates the 9/2± and 11/2± possibilities. The 7/2- state of the

ground state rotational band is the only theoretically reasonable 7/2- state available. This state would decay preferentially to the 3/2- and 5/2- states of the rotational band, which is contrary to observation. The 7/2- assignment is therefore discarded. The only remaining possible assignments are 5/2+ and 7/2+, between which there is no clear choice. If, however, the similarity of the level schemes of Rh^{103} and Ag^{109} is regarded as significant, and the 732-kev level in Ag^{109} is presumed to be the analog of the 538-kev (7/2+) level in Rh^{103}, it seems reasonable to assign the 732-kev level in Ag^{109} as 7/2+.

Transitions were observed from the 860-kev level to levels with spin and parity 3/2-, 5/2-, and 7/2+. Again based on the assumption that these transitions are M1, E1, or E2, the possible spin and parity assignments for the 860-kev level are 3/2+, 5/2±, and 7/2-. The 5/2- assignment is deemed highly improbable for two reasons: (1) The theoretical ratio of the E2 components of the 448-, 553-, and 860-kev transitions is calculated to be 2 : 1 : 80, and the M1 components are all zero because of violation of the strong selection rule $\Delta K \leq L$.[46] The observed transition ratio of 1 : 2 : 0 is therefore a strong argument against the 5/2- assignment. (2) A detectable 141-kev transition to the 719-kev level would be anticipated if the 5/2- assignment were correct. No such transition is observed. For these reasons, the spin assignment 5/2- is discarded as a possibility. The 7/2- possibility has no shell-model analog and would have to be assumed to be the 7/2- rotational state associated with the ground-state rotational band. Such an assignment would adequately explain the existence of the 448- and 553-kev transitions and the absence of the 860-kev transition, but would <u>not</u> explain the observed transitions to the two 7/2+ levels. These latter transitions cannot proceed as normal E1 transitions because of violation of the K selection rule; empirically, E1 transitions which involve $\Delta K = 3$ are retarded by approximately 10^6.

For this reason, the 7/2- assignment is considered to be unlikely. If the 860-kev level were assumed to be 3/2+, the 448-, 553-, and 860-kev transitions would all be E1's. The predicted relative transition probabilities of these three transitions is calculated to be 1 : 7 : 28, respectively, in sharp contrast with the observed values. Also, these E1 transitions would be expected to out-compete the 129- and 773-kev E2 transitions. The only remaining possibility is 5/2+. Such a state would decay to the positive parity states as observed. The transitions to the 3/2- and 5/2- rotational states would be E1 but would be slowed down because $\Delta K \neq 1$, consistent with the fact that their intensities are observed to be comparable to those of the E2 transitions to the two 7/2+ states. Also, since the 860-kev ground-state transition would be M2, it would not be expected to compete measurably with the E1 and E2 gamma transitions which depopulate the 860-kev level. For these reasons, the 860-kev level is assigned to have spin and parity 5/2+. A possible configurational description of this state is $(\quad)^{38}(2p_{1/2})^2(1g_{9/2})^7_{I=5/2}$.

The fact that the log *ft* values 9.9 and 9.5 of the beta transitions to the 3/2- and 5/2- levels, respectively, are much higher than those of normal first-forbidden ($\Delta I = 0, \pm 1$) transitions is a direct consequence of the K = 1/2 character of the final states, i.e., these beta transitions involve $\Delta K = 2$, and thus violate the K selection rule, $\Delta K \leq \Delta I$. The transition retardation factors introduced by violation of ΔK selection rules are almost as large as those introduced by violation of the ΔI rules. It has been found experimentally that most first-forbidden ($\Delta I = 0, \pm 1$) beta transitions which proceed between states with $|K_i - K_f| = 2$ have log *ft* values >8.5. Thus, the log *ft* values of the 0.81- and 0.70-Mev beta transitions are completely consistent with the proposed state assignments.

CHAPTER VI

CONCLUSIONS

This study of the radiations which accompany the decay of the isomers of Pd^{109} has led to the discovery of three previously unobserved energy levels of Ag^{109}. From the observed manner in which these new levels are involved in the Pd^{109} decay scheme, it has been possible to deduce probable spin and parity assignments for all three states. On the basis of these results and the results of similar studies of the excited states of neighboring nuclei, it should eventually be possible for the theorists to arrive at a more detailed, self-consistent interpretation of the level structure of all odd-even nuclides in this mass region.

LIST OF REFERENCES

1. M. G. Mayer and J. H. D. Jensen, Elementary Theory of Nuclear Shell Structure (John Wiley and Sons, New York, 1955).
2. J. P. Elliott and A. M. Lane, Handbuch der Physik (Springer-Verlag, Berlin, 1957), Vol. 39.
3. S. A. Moszkowski, Handbuch der Physik (Springer-Verlag, Berlin, 1957), Vol. 39.
4. A. Bohr and B. R. Mottelson, Kgl. Danske Viedenskab. Selskab, Matfys. Medd. 27, No. 16 (1953) (Ed. 2, 1957).
5. Alder, Bohr, Huus, Mottelson, and Winther, Revs. Modern Phys. 28, 432 (1956).
6. Nuclear Data Sheets (National Academy of Sciences - National Research Council, Washington, D. C., 1958).
7. Strominger, Hollander, and Seaborg, Revs. Modern Phys. 30, 585 (1958).
8. M. G. Mayer, Phys. Rev. 78, 16 (1950).
9. R. H. Nussbaum: Thesis, Amsterdam 1954 (unpublished).
10. M. E. Rose, Beta- and Gamma-Ray Spectroscopy, (Interscience Publishers, Inc., New York; North-Holland Publishing Company, Amsterdam) 1955, Ch. 9.
11. E. Feenberg and G. Trigg, Revs. Modern Phys. 22, 399 (1950).
12. M. G. Mayer, S. A. Moszkowski, L. W. Nordheim, Revs. Modern Phys. 23, 315 (1951).
13. E. Feenberg, Shell Theory of the Nucleus (Princeton University Press, Princeton) 1955, Ch. 4.
14. J. P. Elliott, University of Rochester Department of Physics Report NYO-2271, Sept. 1958 (unpublished).
15. J. P. Elliott and A. M. Lane, loc. cit., p. 256.

16. L. A. Sliv and I. M. Bnad, Leningrad Physico-Technical Institute Report, 1956 [translation: Report 58ICCL1, issued by Physics Department, University of Illinois, Urbana, Illinois (unpublished)].

17. H. Frauenfelder, Beta- and Gamma-Ray Spectroscopy (Interscience Publishers, Inc., New York; North-Holland Publishing Company, Amsterdam) 1955, p. 559.

18. E. Feenberg, loc. cit., p. 65.

19. P. R. Bell, Beta- and Gamma-Ray Spectroscopy (Interscience Publishers, Inc., New York; North-Holland Publishing Company, Amsterdam) 1955,p. 132.

20. C. M. Davisson, Beta- and Gamma-Ray Spectroscopy (Interscience Publishers, Inc., New York; North-Holland Publishing Company, Amsterdam) 1955, p. 24.

21. A. Flammersfeld, Z. Naturf. 7a, 296.

22. U. L. Schindewolf, MIT Progress Report, May 1957, p. 33.

23. J. H. Kahn, ORNL-1089.

24. T. Stribel, Z. Naturf. 12a, 939.

25. E. Amaldi, O. D'Agostino, E. Fermi, B. Pontecorvo, R. Rasetti, E. Segrè, Proc. Roy. Soc. 149A, 522.

26. J. D. Kraus, J. M. Cork, Phys. Rev. 52, 763.

27. W. Rall, Phys. Rev. 70, 112a.

28. I. Bergström, S. Thulin, N. Svartholm, K. Siegbahn, Arkiv Fysik 1, 281.

29. W. W. Meinke, Phys. Rev. 90, 410.

30. D. L. Mock, R. C. Waddel, L. W. Fagg, R. A. Tobin, Phys. Rev. 74, 1536.

31. H. Wäffler, O. Hirzel, Helv. Phys. Acta 21, 200.

32. M. L. Perlman, G. Friedlonder, Phys. Rev. 74, 422.

33. J. Moreau, J. Phys. Radium 15, 380.

34. K. Siegbahn, E. Kondaiah, S. Johansson, Nature 164, 405.

35. A. C. Helmholz, Phys. Rev. 70, 982.

36. A. H. Wapstra, W. van der Eijk, Nuclear Phys. 4, 325 (1957).

37. D. A. Jackson, H. Kuhn, Proc. Roy. Soc. London, 158A, 372.

38. M. F. Crawford, A. L. Schowlow, W. M. Gray, F. M. Kelly, Phys. Rev. 75, 1112.(1949).

39. F. K. McGowan, P. H. Stelson, Phys. Rev. 109, 901 (1958).

40. L. W. Fagg, E. A. Wolichi, R. O. Bondelid, K. L. Dunning, S. Snyder, Phys. Rev. 100, 1299 (1955).

41. G. M. Temmer, N. P. Heydenburg, Phys. Rev. 104, 967 (1956), 95, 861 (1954).

42. T. Huus, J. H. Bjerregaard, B. Elbek, Kgl. Danske Videnskab. Selskab, Mat-Fys. Medd. 30, No. 17.

43. J. deBoer, M. Martin, and P. Marmier, Helv. Phys. Acta. 31, 435.

44. Collected Radiochemical Procedures (Radiochemistry Group J-11) Los Alamos Scientific Laboratory Report LA-1721, December, 1956 (unpublished).

45. A. Bohr, B. R. Mottleson, Kgl. Danske Videnskab. Selskab, Mat-Fys. Med. 27, No. 16.

46. G. Alaga, K. Alder, A. Bohr, and B. R. Mottelson, Kgl. Danske Videnskab. Selskab, Mat-Fys. Medd. 29, No. 9.

IMPORTANT!

Special care should be taken to prevent loss or damage of this volume. If lost or damaged, it must be paid for at the current rate of typing.

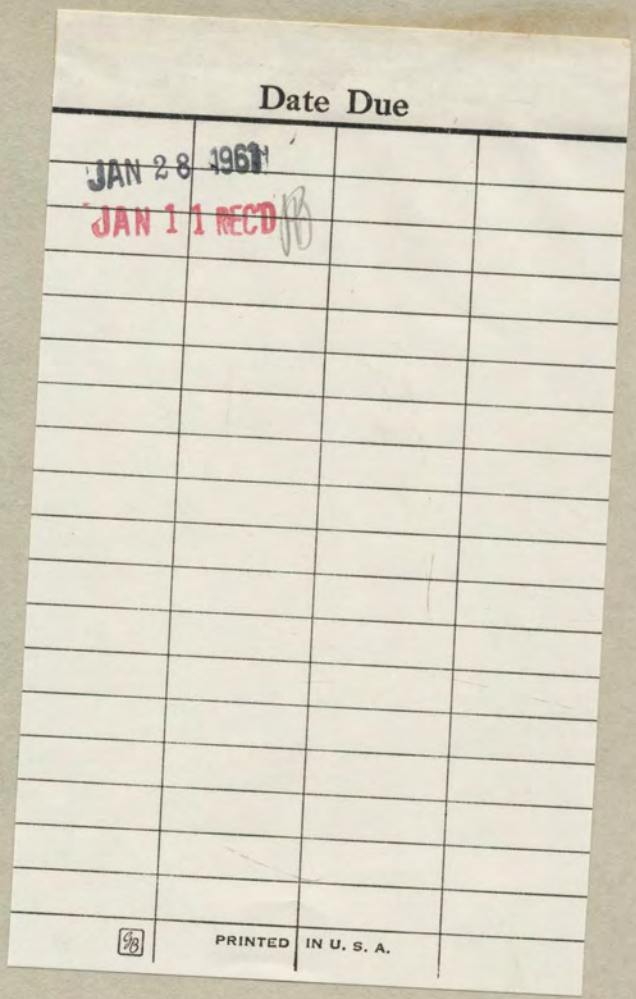

Date Due

JAN 28 1961

JAN 11 RECD

PRINTED IN U. S. A.